THE ASTRONOMICAL JOURNAL, 123:304–327, 2002 January

THE YOUNG CLUSTER IC 5146

G. H. HERBIG AND S. E. DAHM
Institute for Astronomy, University of Hawaii, 2680 Woodlawn Drive, Honolulu, HI 96822
Received 2001 August 13; accepted 2001 September 26

ABSTRACT

The B0 V star BD +46°3474 lies near the front surface of a dense molecular cloud and illuminates the emission/reflection nebula IC 5146. The HAeBe variable BD +46°3471 is embedded in the same cloud, about 10′ (3.5 pc) away. CCD photometry in *BVRI* (to $V = 22$) and in *JHK* (to about $K = 16.5$) has been obtained for the young clusters surrounding each of these two bright stars. Some 100 emission-Hα stars brighter than $R = 20.5$ have been found in the area, most of them in IC 5146. (Among these are two that have spectra resembling a high-excitation Herbig-Haro [HH] object plus a stellar continuum.) A distance of 1.2 kpc follows from the photometry of several late-type IC 5146 cluster members; the average extinction from 38 stars classified spectroscopically is $A_V = 3.0 \pm 0.2$ mag. Although optical photometry is available for 700 stars in the IC 5146 field, only about half (including all the Hα emitters) lie above the main sequence, while a substantial fraction of these are estimated to be foreground. A number of such interlopers have been identified on the basis of proper motion or abnormally low A_V. The age distribution of the Hα emitters has been estimated by reference to several sets of theoretical isochrones. There is substantial disagreement, but the median age does appear to be near 1 Myr. The spectrum of +46°3474 is unexceptional except for an unusually low $v \sin i$ (10 km s^{-1}), but +46°3471 has a complex emission plus absorption spectrum. Our interpretation of the structure of IC 5146 on the basis of optical and radio radial velocities follows a proposal by Roger & Irwin in 1982, namely, that +46°3474 formed near the near surface of the present cloud and evacuated a blister cavity out of which gas and dust are now flowing through a funnel-shaped volume in the approximate direction of the Sun. It is suggested that the IC 5146 cluster stars formed in a dense foreground section of the molecular cloud that was dissipated following the appearance of +46°3474.

Key words: open clusters and associations: individual (IC 5146) — stars: emission-line, Be — stars: formation — stars: pre–main-sequence

On-line material: machine-readable tables

1. INTRODUCTION

IC 5146 is the emission/reflection nebulosity surrounding the early B-type star BD +46°3474. The star is embedded in a molecular cloud at the eastern extremity of a 2°-long dark filament that has been mapped in CO and CS by Lada et al. (1994). A number of faint emission-Hα stars in IC 5146 had been found at Lick in the early 1950s, but W. Baade's (unpublished) discovery of a clustering of faint red stars around +46°3474 provided the impetus for modern investigations of the stellar content of IC 5146, beginning with Walker's (1959) *UBV* photoelectric and photographic photometry to about $V = 17$. Elias (1978) added near-IR photometry of the brighter stars in the area, but the deepest photometry published to date is that of Forte & Orsatti (1984), who measured photographic *UBVRI* magnitudes for about 1000 stars in the area to about $V = 20.5$. The present investigation is intended to go somewhat deeper in both *BVRI* and *JHK*, to supplement the photometry with classification spectroscopy of many cluster stars and to discuss the many Hα-emission stars that we have found in and around IC 5146.

Figure 1 shows the region in blue light, as photographed by Baade in 1951 with the 5 m Hale Telescope. The HAeBe star +46°3471 lies about 10′ to the west of IC 5146 and in the same cloud; it is the nebulous star near the right edge of Figure 1. There is a small secondary clustering of pre–main-sequence stars around +46°3471 for which we have obtained *BVRI* and *JHK* photometry and some spectroscopy, to be described in § 4. The FU Ori–like variable V1735 Cyg, discovered by Elias (1978), lies in the same dark lane about 1° from IC 5146.

2. OBSERVATIONS

2.1. *Optical Photometry*

Our *BVRI* photometry consists of exposures obtained in 1993 June and in 1999 September at the f/10 focus of the University of Hawaii (UH) 2.2 m telescope on Mauna Kea and centered on BD +46°3474 and BD +46°3471. In 1993 the observer was B. Patten, and the detector was a 2048^2 CCD with 24 μm pixels. Our more extensive 1999 data employed the same detector with a different filter set that has slightly different transmission characteristics, resulting in magnitudes and colors differing by a small zero-point offset. The scale was 0.″22 pixel^{-1}, the field about 7.′5 in diameter. In both series three exposures of 5 (or 10), 60, and 300 s were made. Conditions were photometric on both occasions, with average seeing of about FWHM = 0.″9. This photometry was reduced to the BVR_CI_C system defined by Landolt (1992) standard fields, and employed the IRAF DAOPHOT package, with aperture photometry with point-spread function fitting by the PHOT, PSF, and ALLSTAR tasks. (Hereafter we omit the subscript on R_C and I_C.) Over 700 stars in each of the fields were measurable in all four bandpasses. The limiting magnitude is about $V = 22.0$, with completeness expected to $V = 20.5$. Figure 2 shows in the V, $V-I$ plane all the stars measured, but with no allowance for reddening. The solid line is the Pleiades main sequence for a

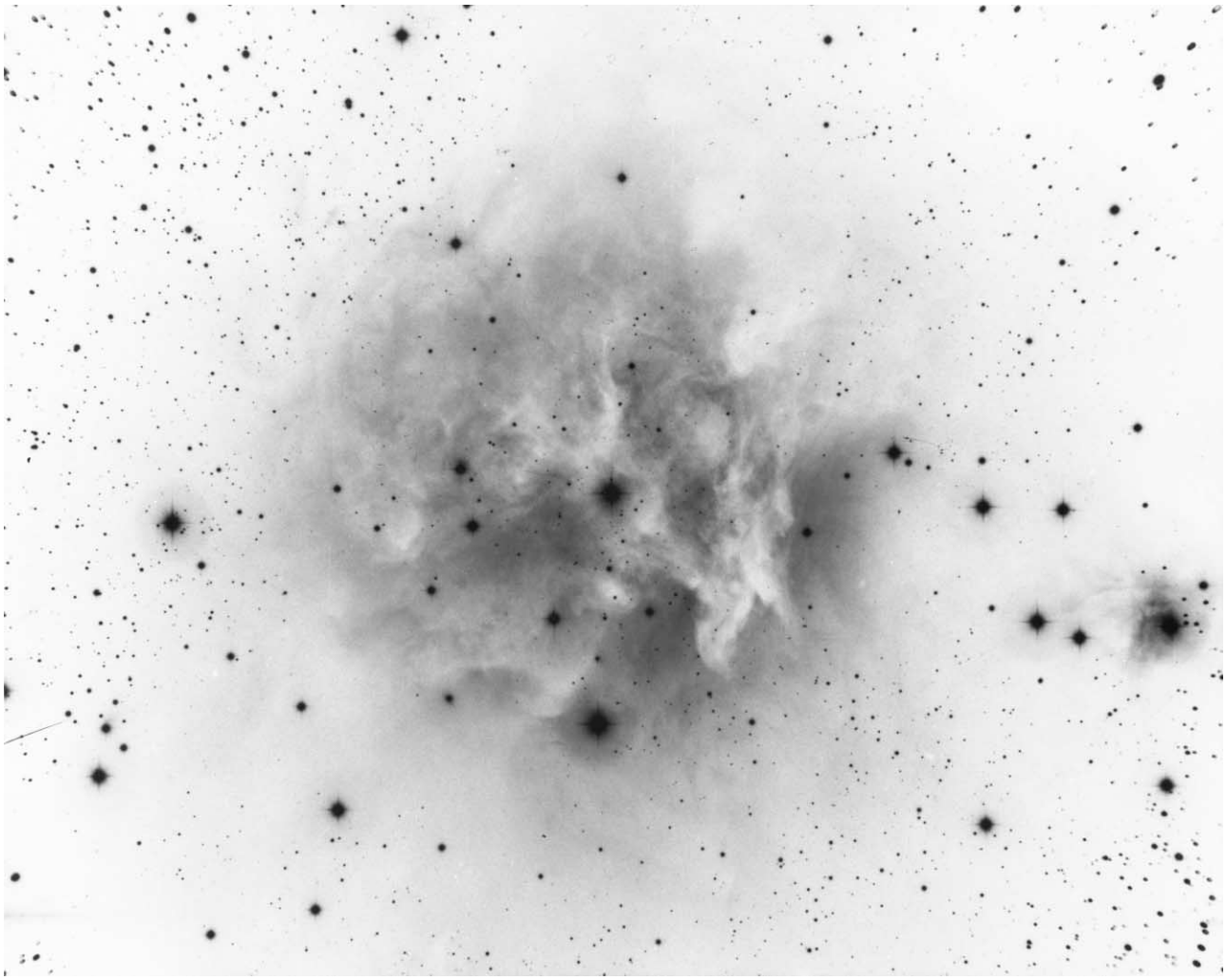

FIG. 1.—IC 5146 region, from a photograph in blue-violet light obtained by W. Baade with the 5 m Hale telescope on 1951 August 11; the same negative was used for Fig. 3 of Walker (1959). It is reproduced with permission of the Observatories of the Carnegie Institution of Washington. The area shown is about $20' \times 16'$; north is at the top and east to the left. BD +46°3474 is central in the nebulosity; the equally bright star at the southern edge of the nebula is +46°3475, a foreground G0 V. BD +46°3471 is the nebulous star near the right-hand edge of the figure.

distance of 1.2 kpc. Table 1 contains the detailed results for about 380 stars (of the 700) that we believe lie above that main sequence (as explained in § 3.1), while Table 2 contains similar data for the area centered on +46°3471. The J2000.0 coordinates in Tables 1 and 2 are based on reference stars from the *HST* Guide Star and USNO-A catalogs.

The 1993 images of the +46°3471 field suffered from a transient bias ramping problem that affected rows containing bright stars at the DN ≈ 20–30 level, so the final magnitudes for that area are based only on the 1999 exposures.

Figure 3 displays the internal errors in our optical and near-infrared (§ 2.2) photometry.

Forte & Orsatti (1984) derived *UBVRI* magnitudes for over 1000 stars in the IC 5146 area from photographic plates obtained at the prime focus of the KPNO 4 m Mayall telescope. Some 200 stars common to the two photometries could be identified from their published pixel coordinates. The panels of Figure 4 show the differences between the two series in V, $B-V$, $V-R$, and $V-I$. Similarly, Figure 5 shows the differences between our V and $B-V$ values and the photoelectric measures of Walker (1959).

2.2. *Near-Infrared Photometry*

Two sets of *JHK* observations were obtained by Dahm in 1999 July and September at the UH 2.2 m telescope with the Quick Infrared Camera (QUIRC). The scale is $0''.189$ pixel^{-1}, and the field of view approximately $3'.2$ in diameter. The new Mauna Kea filters installed in QUIRC have somewhat different transmission profiles than their Johnson, CIT, or Arizona counterparts. The Mauna Kea *J*-band filter cuts off near 1.33 μm, while the *K* filter cuts off sharply near 2.35 μm. Three dithered images (exposures 10 and 60 s) were taken in each of five fields centered near BD +46°3474 and BD +46°3471. The area covered as a result was about $6'.4$ in diameter. After each program exposure, an off-field image was taken several arcminutes away to create a median-filtered sky frame. Faint UKIRT and ARNICA standards from Hunt et al. (1998) were observed regularly throughout the night.

An automated IRAF script written by W. D. Vacca that blanks out stars and generates median-combined sky and flat-field frames was used for initial reductions. Aperture photometry on the resulting sky-subtracted and flattened-

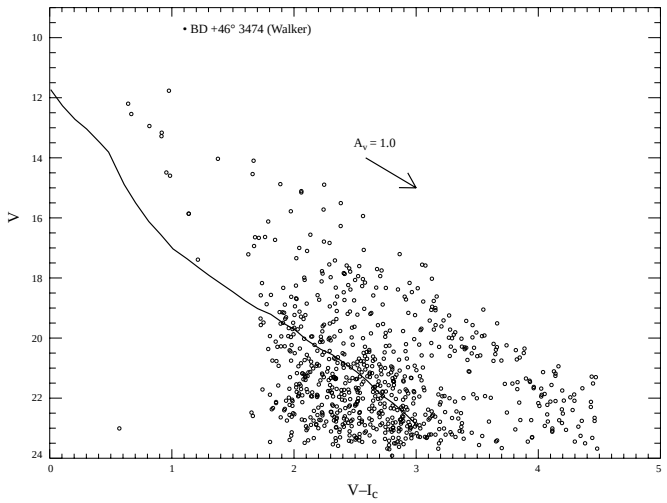

FIG. 2.—Plot of the observed V vs. $V-I$ values of all the stars measured in *BVRI*. There has been no allowance for (interstellar) extinction. The Pleiades main sequence is shown for an assumed distance of 1.2 kpc. BD+ 46°3474 (*filled dot*) was too bright for our *VI* photometry; the position plotted is inferred from Walker's V, $B-V$ and Kenyon & Hartmann (1995) normal colors, and the assumption of normal reddening.

field images was then carried out with PHOT/DAOPHOT. All objects having signal-to-noise ratios of less than 3 in any bandpass were discarded. The statistical errors for the resulting J and $J-K$ are shown in Figure 3. The K magnitude limit is near $K = 16.5$.

Over 800 NIR sources were identified at or above the 3 σ level in all three bandpasses. About 150 of these that lay below the V, $V-I$ main sequence (explained in § 3.1) were plotted on a $J-H$, $H-K$ diagram, where it was found that many scattered outside the conventional reddening band. To be sure that some error in our photometric system was not responsible, our *JHK* observations of two fields in IC 348 that had been taken during the same run with the same equipment were reduced in the same way. These results were compared with the SQIID data for IC 348 of Lada & Lada (1995). No systematic differences were found: the differences between the two data sets had standard deviations of 0.22, 0.12, and 0.12 mag for J, H, and K, respectively. Furthermore, we found no systematic dependence of the QUIRC $J-H$ and $H-K$ errors on color. We therefore believe that most of the $J-H$, $H-K$ scatter in this below–the–main-sequence sample that is not attributable to reddening is caused by a combination of our own errors with those

TABLE 1
PRE–MAIN-SEQUENCE CANDIDATES IN IC 5146

Star	IHα	α (21 53 +)	δ (47 +)	V	$B-V$	$V-R$	$V-I$	R	$R-I$	J	$J-H$	$H-K$	W(Hα)
1.....	...	4.60	12 54.8	16.46	1.17	0.74	1.57	15.72	0.83	...	...	...	...
2.....	...	4.84	16 58.4	20.24	2.15	1.31	2.79	18.93	1.48	...	...	...	...
3.....	...	5.06	12 12.3	15.83	2.14	1.31	2.23	14.52	0.91	...	...	...	...
4.....	...	5.27	16 15.3	14.74	0.77	0.41	0.87	14.33	0.46	...	...	...	...
5.....	...	5.28	15 52.6	21.33	1.83	1.36	2.99	19.97	1.63	...	...	...	...
6.....	...	5.32	17 41.2	16.31	2.29	1.40	2.61	14.91	1.21	...	...	...	...
7.....	...	5.96	17 48.0	17.14	2.08	1.29	2.64	15.85	1.35	...	...	...	...
8.....	...	6.06	17 36.6	15.77	2.07	1.29	2.22	14.48	0.93	...	...	...	...
9.....	...	6.10	17 41.4	21.44	2.41	1.54	3.41	19.90	1.87	...	...	...	...
10.....	...	6.32	15 04.9	19.43	1.69	0.96	2.33	18.48	1.37	...	...	...	...

NOTES.—Table 1 is presented in its entirety in the electronic edition of the Astronomical Journal. A portion is shown here for guidance regarding its form and content. Units of right ascension are hours, minutes, and seconds, and units of declination are degrees, arcminutes, and arcseconds (J2000.0).

TABLE 2
PRE–MAIN-SEQUENCE CANDIDATES IN THE AREA OF BD +46°3471

Star	IHα	α (21 52 +)	δ (47 +)	V	$B-V$	$V-R$	$V-I$	R	$R-I$	J	$J-H$	$H-K$	W(Hα)
400....	...	13.35	17 26.3	23.59	2.76	1.14	3.23	22.45	2.09	...	...	...	...
401....	...	13.96	10 11.8	22.82	1.39	1.27	3.11	21.55	1.84	...	...	...	...
402....	...	14.27	16 03.3	23.00	1.50	1.40	3.24	21.60	1.84	...	...	...	...
403[a]...	...	14.29	12 11.9	20.47	1.80	1.18	3.35	19.29	2.17	...	...	...	...
404....	...	14.37	11 12.5	18.03	1.02	0.61	1.21	17.42	0.60	...	...	...	...
405....	...	14.43	13 28.7	23.13	1.65	1.35	3.20	21.78	1.85	...	...	...	...
406....	...	14.52	12 57.6	23.68	0.94	1.57	3.54	22.11	1.97	...	...	...	...
407....	174	14.54	14 24.2	16.75	1.35	0.87	1.87	15.88	1.00	...	...	...	7
408....	...	14.58	16 42.1	19.94	2.21	1.46	2.83	18.48	1.37	...	...	...	...
409....	...	14.77	14 01.3	22.63	1.96	1.39	3.17	21.24	1.78	...	...	...	...
410....	...	14.81	14 10.4	15.62	0.97	0.61	1.16	15.01	0.55	...	...	...	...

NOTES.—Table 2 is presented in its entirety in the electronic edition of the Astronomical Journal. A portion is shown here for guidance regarding its form and content. Units of right ascension are hours, minutes, and seconds, and units of declination are degrees, arcminutes, and arcseconds (J2000.0).

[a] Detected proper motion, most likely foreground.

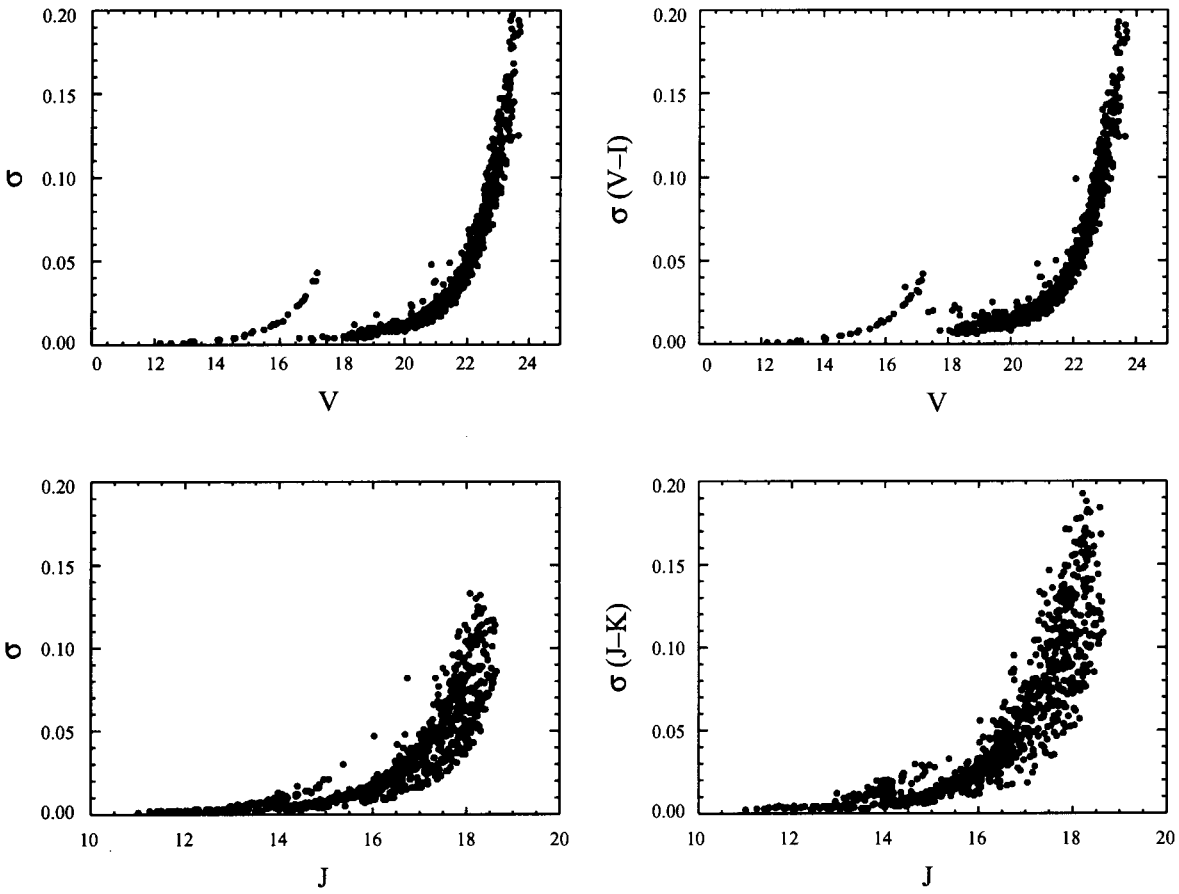

FIG. 3.—Internal errors of the present V, $V-I$, J, and $J-K$ photometry, shown separately for the short and long exposures

quoted by Lada & Lada and by the larger photometric uncertainties of these faint sources.

2.3. *Spectroscopy*

Spectrograms of over 60 stars in an area centered on BD +46°3474 and of about 20 around BD +46°3471 were obtained in 1994 October with the Multi-Object Spectrograph (MOS) at the 3.6 m Canada-France-Hawaii Telescope. These spectra covered the range 5850–7050 Å at either of two dispersions: 1.55 or 3.6 Å pixel^{-1}. They were classified with reference to standards in the spectral atlases of Allen & Strom (1995), Kirkpatrick, Henry, & McCarthy (1991), and Jacoby, Hunter, & Christian (1984). The red region is very suitable for classification of K- or M-type stars, where the strength of the TiO structure 6200–6350 Å, the Ca I lines 6102, 6122, 6160 Å, and the Na I D lines were the main criteria. Classification of F and G stars is more difficult in the red at this resolution; the Ca I lines, Na I D were most useful, plus Hα when it was not in emission or filled in. For late-B types, He I 5876 and 6678 Å were the main indicators. Uncertainties in the assigned types are about 1–2 subclasses for the later types and 2–3 for those earlier than G5.

Additional slit spectrograms were obtained for many of the brighter stars in and around IC 5146 in 1999 October with the High Angular Resolution Spectrograph (HARIS) with the Tektronix CCD at the UH 2.2 m telescope. These covered the 3800–5900 Å region at a resolution of about 500, and were particularly useful for the earlier type stars. In all this spectroscopy, the nebular background was subtracted by sampling the sky on either side of the star spectrum. All these spectral classifications are collected in Table 3.

HIRES spectrograms (resolution 45,000) of +46°3474 and +46°3471 were obtained at the Keck I telescope[1] and will be described in §§ 3.7 and 4.3.

2.4. *The* Hα*-Emission Stars*

About 20 Hα-emission stars in this general area were found by Herbig (1960a) in the 1952–1959 photographic survey carried out with a grism arrangement at the Lick Crossley 0.91 m reflector. The limiting magnitude was about $R = 17.0$, judging from modern CCD photometry of 12 of the same stars in the somewhat smaller area investigated here. The search was resumed in 1990 with a similar spectrograph at the f/10 focus of the UH 2.2 m reflector on Mauna Kea. The detector was a 800^2 CCD, and the dispersion 6.6 Å pixel^{-1}. That survey was repeated in 1996 with the same instrument, but now with different optics imaging on the central 1024^2 pixels of a Tektronix CCD; the dispersion was 3.85 Å pixel^{-1}. Some 80 additional Hα emitters brighter than about $R = 20.5$ were found in IC 5146, and about 10 around BD +46°3471. The continua of these stars were suf-

[1] The W. M. Keck Observatory is operated as a scientific partnership among the California Institute of Technology, the University of California, and the National Aeronautics and Space Administration. The Observatory was made possible by the generous financial support of the W. M. Keck Foundation.

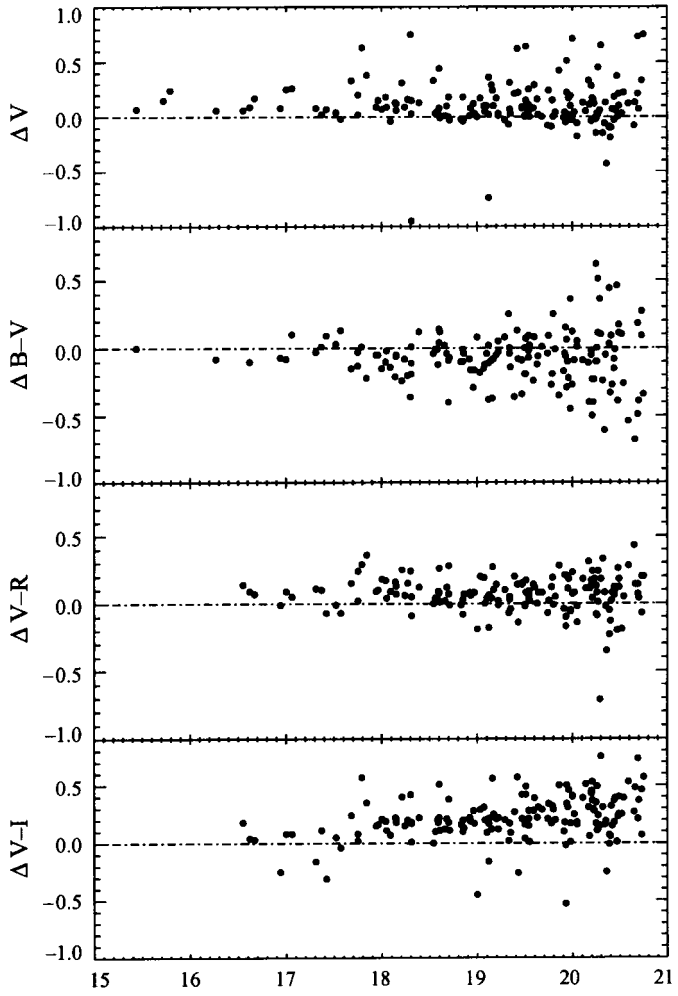

FIG. 4.—Residuals: the V, $B-V$, $V-R$, and $V-I$ values of this investigation *minus* the photographic values of Forte & Orsatti (1984), all as a function of (our) V.

ficiently well defined for the equivalent width of the emission to be measured. T Tauri stars (TTSs) are conventionally separated into two classes (WTTS and CTTS) at $W(\mathrm{H}\alpha) = 10$ Å. Our limiting $W(\mathrm{H}\alpha)$ is about 3 Å, compared with about 10 Å for conventional photographic surveys, so that these discoveries extend well into the WTTS domain.[2]

All stars brighter than about $V = 22$ in Table 1 were examined specifically on the grism frames, and if no emission was present on a detectable continuum, that star was marked "<5" Å in Table 1. All stars in Table 2 brighter than $R = 20.0$ were similarly examined. If the continuum was lost in the noise, if there was some interference by nearby spectra, or if the star fell outside the grism field, the $W(\mathrm{H}\alpha)$ column is left blank. In Tables 1 and 2, "em" appears in those cases where only the emission line was detectable above the sky noise, or where emission was detected but the continuum level was confused by an overlapping spectrum.

[2] Note that these equivalent widths are with respect to the continuum interpolated across the line, i.e., there has been no allowance for filling-in of the underlying absorption line, which is estimated to amount to about 2.7 Å at G5 V but diminishes to about 0.5 Å at M3 V (Herbig, Vrba, & Rydgren 1986).

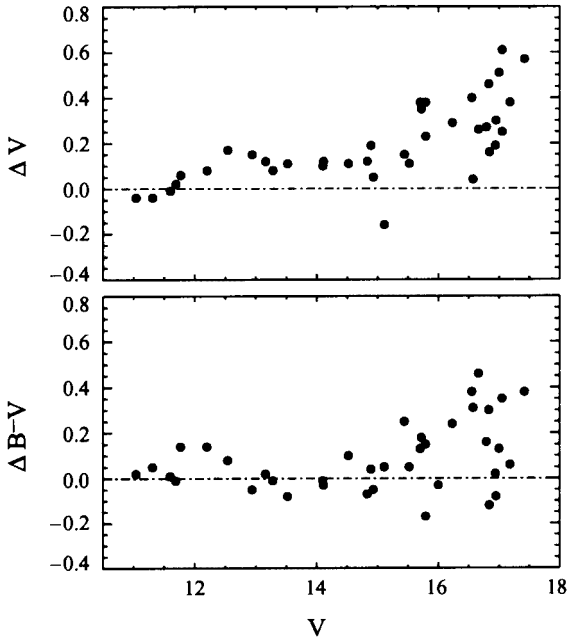

FIG. 5.—Residuals: the V and $B-V$ values of this investigation *minus* the photoelectric values of Walker (1959), both as a function of (our) V.

IHα numbers (formerly IfAHα) are assigned in Tables 1 and 2 to the grism detections, in continuation of the numbering system of Herbig (1998).

The distribution of the Hα emitters over IC 5146 is shown in Figure 6, where the positions of CTTSs are marked by large crosses and WTTSs by smaller ones. Their distribution is not centered on BD +46°3474: there is a clear preference for the regions east and especially southeast of the center of the bright nebulosity. An interpretation will be offered in § 3.9.

3. IC 5146: THE CLUSTER AND THE NEBULOSITY

3.1. *Distance, Color-Magnitude Diagram, Variable Stars*

Walker's (1959) estimate of the distance of IC 5146 was based on his *UBV* colors of four bright late-B stars (W35, W62, W64, and W76); BD +46°3474 was not used in case it may already have evolved off the main sequence. The resulting distance of 1.0 kpc depended on the zero-age M_V values of Johnson & Hiltner (1956). Elias (1978), on the basis of Walker's *BV* data and his own NIR photometry, obtained a distance of 900 pc, now including +46°3474 but not W76, and assuming the main-sequence M_V values of Blaauw (1963). Since those early investigations improved normal colors and absolute magnitudes have become available, including a *Hipparcos*-based recalibration of the B- to F-type main-sequence by Jaschek & Gómez (1998).

We have followed the same procedure using our own *BVRI* data for the B8, B9 stars W35, W62, W64, which we assume define the main sequence of IC 5146. Normal colors were drawn from Straižys (1992) and from Kenyon & Hartmann (1995), and the M_V values from Jaschek & Gómez (1998) and Schmidt-Kaler (1982), while color excesses were converted to A_V values by the normal reddening relationships $A_V = 3.08E(B-V) = 2.43E(V-I)$. The resulting distance of IC 5146 depends upon which set of M_V values is used, but not upon whose set of normal colors. Extinction

TABLE 3
SPECTRAL CLASSIFICATIONS

Table 1 or 2	Walker (No.)	Type	$W(\mathrm{H}\alpha)$	Table 1 or 2	Walker (No.)	Type	$W(\mathrm{H}\alpha)$	Table 1 or 2	Walker (No.)	Type	$W(\mathrm{H}\alpha)$
8	...	G9	...	165	...	M2	2	369	W68	K6	44
21	W22	K5	2.0	172	W39	K1	6	372	W69	G7	<5
22[a]	W23	G5	<5	188[a,b]	W41	M1	<5	373[a]	W70	G2	<5
32	...	K4	4.5	194	W44	K1	<5	162	W37	G4	abs
39[a]	...	M1	...	203	...	G8	<5	306[a]	...	K8	<5
46[a]	W24	K8	<5	210	W46	K0	28	4[a]	...	G3	...
53	...	G8	<5	215	...	K5	24	488	...	G5	<5
55	W28	K5	1.5	247	W49	K3	1.5	497	W1	K1	50
67	...	K0	2	249	...	K7	22	514	L236	K0	28
80	...	M1	4	251	W50	G3	<5	536[a]	...	A5	...
83	W30	K7	300	268	W53	B8	<5	545	...	G5	abs
100	...	G8	1:	291	L247	K6	16	547	L239	K7	35
108	W31	K8	2	308	L248	K5	46	551[a]	...	F9	...
116	L243	K7	49		W55	K8	<5	579[a,b]	...	M0.5	<5
129	W32	K2	<5	315	W56	K0	<5	596[a]	W8	F0	...
	W34	G7	abs	332[a]	W58	G6	abs	597	L240	K7	125
140	W35	B9	<5	346	W61	K6	60	625[a]	W11	F5	...
144	...	F5	2:	350	W62	B8	abs	672[a]	W14	F5	...
148	...	K4	3.5	352	W63	F8	abs	673	W13	F7	...
154	W36	K1	17	357	W64	B9	abs	675[a]	...	F8	...
164	...	M4	10		W65	K0	abs				
	W38	F9	abs	3	W66	F0	1.6				

[a] Probably foreground: small A_V.
[b] Probably foreground: significant proper motion.

obtained from $B-V$ excesses gives 1.4 kpc for the Schmidt-Kaler M_V values and 1.1 kpc for the Jaschek & Gómez values. Similarly, the $V-I$ excesses give 1.3 and 1.0 kpc, respectively. (The old Johnson & Hiltner M_V values would have led to values of 0.9 to 1.0 kpc, thus explaining the lesser distances obtained by Walker and by Elias.) In what follows we adopt the compromise distance of 1.2 kpc.

But a caution: such calculations, in the words of Jaschek & Gómez (1998), assume that "a strict relation exists between luminosity class and absolute magnitude" as if the luminosity class "were a coded absolute magnitude." They conclude, from a discussion of *Hipparcos* distances of MK standard stars, that this comfortable assumption is not correct: "the relation between absolute magnitude and luminosity class is only a statistical one, which has a large intrinsic dispersion." They find that, for a given main-sequence B spectral subtype, M_V is distributed around its mean with standard deviation of about 0.55 mag (Gómez et al. 1997). Thus for our sample of three stars drawn from such a population, we can expect a σ of about $0.55/3^{1/2}$ mag, which alone translates into an uncertainty in the distance of ± 180 pc even in the absence of the other uncertainties.

W53 (B8) lies near the main sequence but has not been used for distance estimates because these optical and NIR colors may be anomalous (Elias 1978), although Elias's colors may be affected by inclusion of the star's two close companions.

Given the distance of 1.2 kpc, individual extinction corrections can be obtained for the 46 stars of known spectral type, of which 38 are believed to be cluster members (see § 3.2). If we assume all the latter to lie on the main sequence, then an average A_V of 3.0 ± 0.2 mag follows. That average has been applied to all others, although it is likely that some fainter cluster members are more deeply embedded than this average. Figure 7 is the resulting V_0, $(V-I)_0$ diagram. The solid line represents the Pleiades main sequence. Only stars lying above that line are plotted (and, as explained, only they are listed in Table 1). Filled blue points are stars of known spectral type. Crosses mark stars having Hα in emission. Filled reds represent stars of unknown type, corrected for reddening by assuming that $A_V = 3.0$ mag and, unless crossed, having $W(\mathrm{H}\alpha) < 5$ Å. Open black circles represent stars having continua below the grism threshold (or that fall outside the area of the grism survey).

A number of stars that showed significant brightness changes between the two epochs are so indicated in Tables 1 and 2. Walker (1959) listed some 20 stars in the area that he regarded as variable. They are listed in Table 4, together with their *BVRI* ranges if they fell within our photometric area. Of the 15 such variables that we locate above the main sequence, 14 have Hα in emission, as would be expected. We confirm that the only one that does not (Walker 21 = our 334) is indeed variable. It may be a foreground variable of another type.

3.2. *Foreground Contamination*

Contamination of the color-magnitude diagram by foreground stars is a concern for a cluster as distant as IC 5146. There may also be contamination by background stars if the molecular cloud is not completely opaque. To estimate the foreground contribution, the main-sequence luminosity function tabulated by Jahreiss & Wielen (1997) was adopted. The dependence of $V-I$ on M_V was taken from the *Hipparcos* data for the brighter stars and from the compilations of Leggett, Allard, & Hauschildt (1998) and Leggett et al. (2000) for the fainter. The luminosity function was summed over distance in shells of equal spacing, in a cone terminating in an area of $7' \times 7'$ at 1.2 kpc. It was assumed

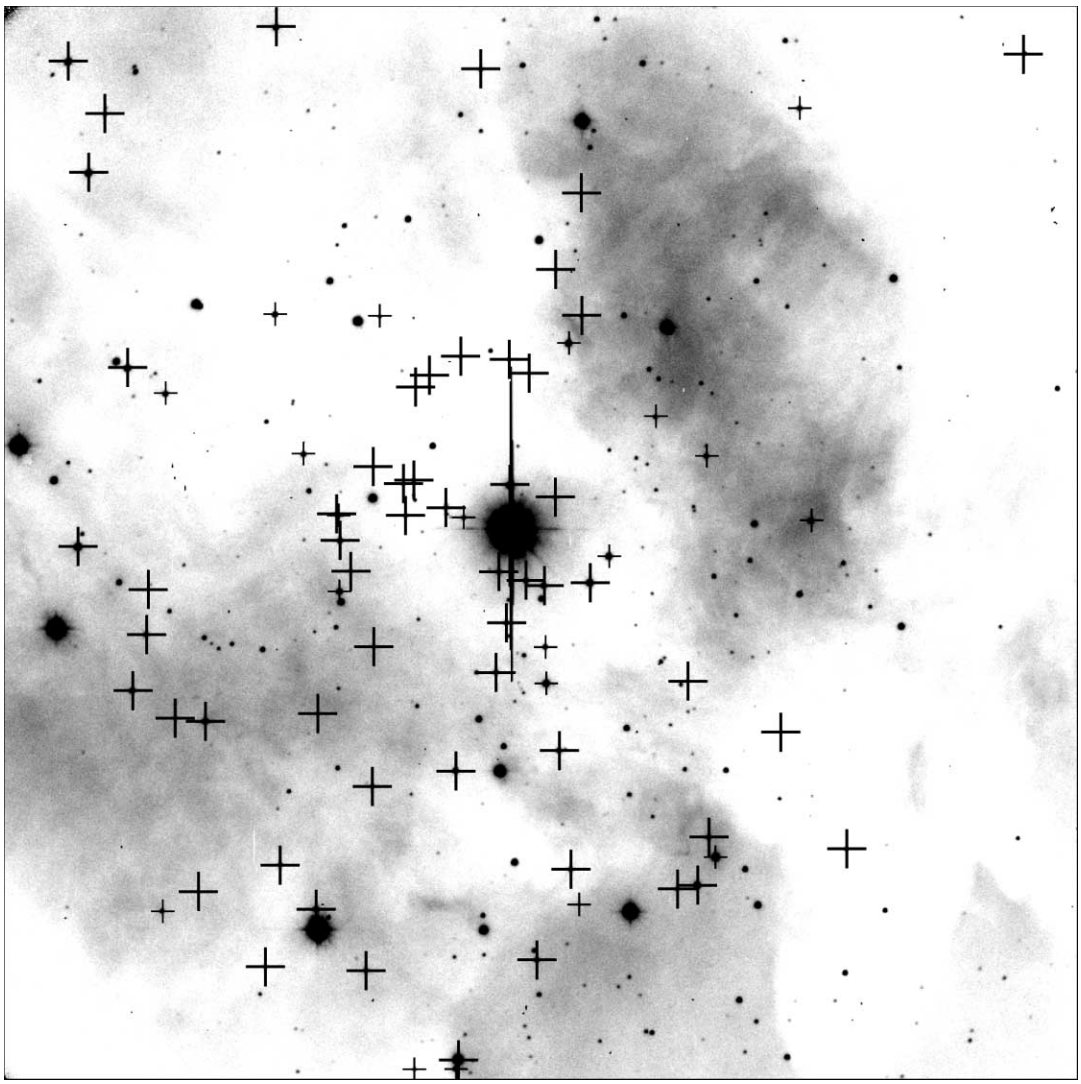

FIG. 6.—Distribution of Hα-emission stars in the field of IC 5146 (the area shown is about 350″ on a side; north is at the top, and east to the left). Large crosses mark those having $W(\mathrm{H}\alpha) \geq 10$ Å, small crosses those with $W(\mathrm{H}\alpha) < 10$ Å. Three additional stars lie off the southern edge of this figure, and one off the eastern edge.

that A_V increased uniformly with distance, but no allowance was made for variation of the local star density along the line of sight.

Figure 8 shows the predicted V, $V-I$ diagram of the foreground. It was assumed that A_V increased with distance at a rate of 2.0 mag kpc^{-1}, but then all the foreground stars were dereddened for an average A_V of 3.0 mag, as was done for all stars of unknown spectral type in constructing Figure 7. The number of stars predicted to fall in each box of dimensions 1.0×0.1 mag is shown at the position of that box. The solid line is again the Pleiades main sequence of Figure 7. A rather similar result would have been obtained if the Kroupa (1995) luminosity function had been used; it differs from the Jahreiss-Wielen tabulation by a factor of less than 2 at common values of M_V.

The densest concentration of points near the main-sequence line in Figure 8, in the interval $V-I = 1.3$ to 2.2, is contributed by M0–M5 dwarfs beyond 500 pc. Some of those foreground M dwarfs may have grism-detectable Hα emission and thus will contribute to our WTTS count.

Table 5 gives, for color intervals of 0.3 mag, the numbers of stars having detectable or undetectable Hα emission on the grism spectrograms and also the predicted number of foreground stars above the main sequence (for two values of A_V kpc^{-1}). The latter were extracted from the numbers of Figure 8. Details are given at the foot of the table. It is numbers such as those in columns (7) or (8) that should be subtracted from the totals of nonemission stars in columns (4) and (5). Thus a substantial fraction of the nonemission stars above the main sequence of Figure 7 must not be cluster members. However, in IC 348 the fraction of stars having Hα emission is known to increase as $W(\mathrm{H}\alpha)$ decreases, so it is possible that in IC 5146 some column (4) stars simply have emission below the grism threshold.

Reddened K- and M-type giants in the background could fall at any V_0 level in Figure 7. We do not attempt to model their contribution for lack of information on the opacity of the cloud behind the cluster.

Some foreground interlopers can be recognized if they have large proper motions with respect to a reference frame defined by known cluster members, in this case by the

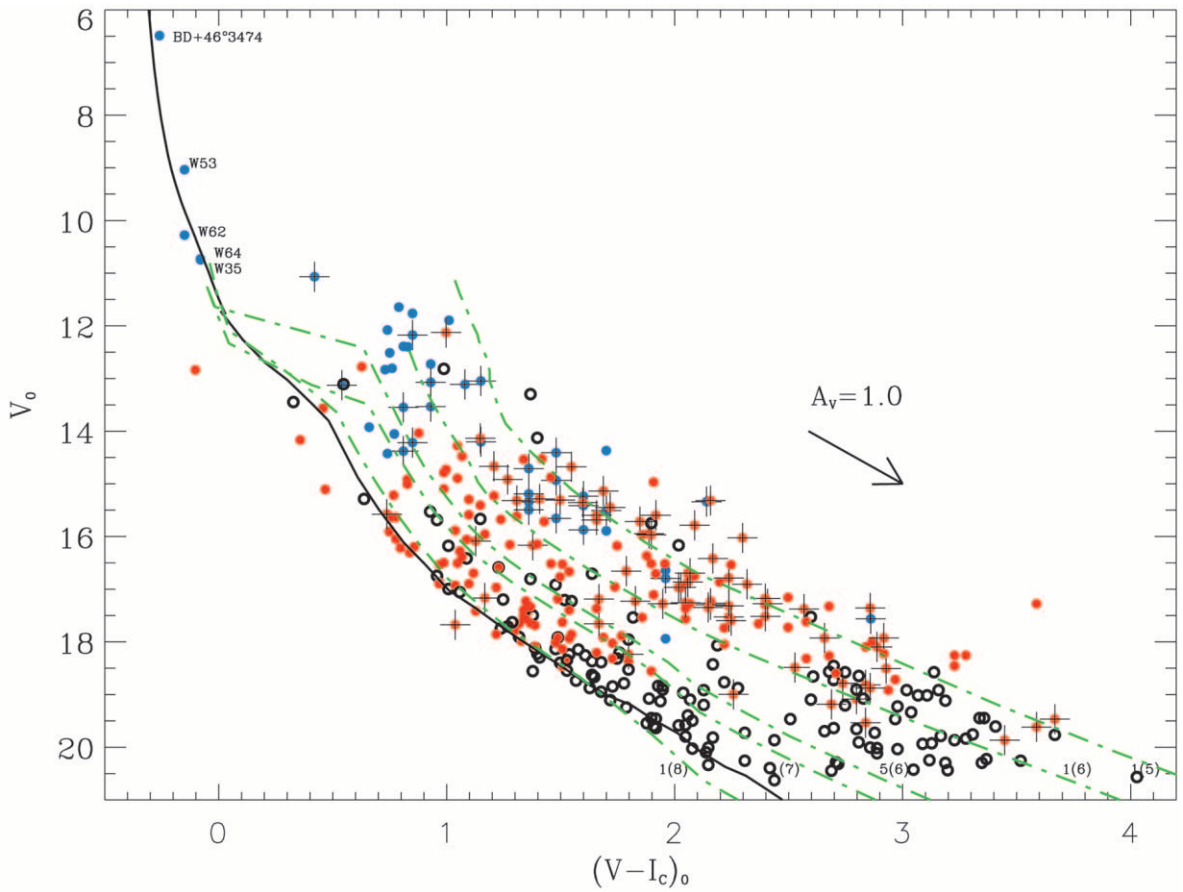

FIG. 7.—Color-magnitude diagram: a plot of V_0 vs. $(V-I)_0$ for those stars in Fig. 2 that lie above the Pleiades main sequence, following correction for extinction. Hα emitters are marked by crosses; if uncrossed, W(Hα) is less than 5 Å. Filled blue points indicate stars of known spectral type. Filled red points mark those of unknown type, and hence corrected for extinction by the mean cluster A_V. Open black circles indicate a star either too faint to determine whether Hα is present or not, or one that lies outside the area surveyed. The interesting stars W46 and W66, mentioned in the text, are plotted at (12.17, 0.85) and (11.07, 0.42), respectively. Star 312 is the point at (17.28, 3.59).

known Hα emitters. Two R-band images of the IC 5146 field with a time separation of 6.5 yr were examined. Although the shape of the stellar PSFs differs between the epochs on account of seeing and instrumental differences, the centroid positions ought to be stable at a certain level. That level was determined by measuring centroid shifts for 650 stars in the IC 5146 field (and 780 around BD +46°3471). The standard deviation from the mean is about 0.″05. Shifts between the two frames of about 0.″1 were at the threshold of detection by blinking, which corresponds to a velocity of 88 km s^{-1} at 1200 pc.

Nine stars located above the main sequence in IC 5146 were found to shift between the frames by 0.″14 to 0.″50, corresponding to annual proper motions of 0.″022 to 0.″076 yr^{-1}. A similar search around +46°3471 detected 12 more stars having shifts ranging from 0.″11 to 0.″40. None have detectable Hα emission. Two of them, stars 188 and 579, have known spectral types and had already been recognized as foreground from their low A_V values. Of all the stars of known type listed in Table 3, 15 have $A_V < 1.0$ mag and hence are probably in the foreground. They are so indicated in Tables 1, 2, and 3.

3.3. *Infrared Magnitudes and Colors*

$H-K$ (or better, $K-L$) excess, is regarded as a disk indicator. Kenyon & Hartmann (1995, Fig. 4) showed that in the Tau-Aur TTSs there was a striking rise in W(Hα) as $K-L$ increased beyond about 0.3 mag. Hartmann (1998, p. 123) interpreted this break as the boundary between WTTSs (Hα largely chromospheric) and CTTSs (Hα dominated by accretion). Haisch, Lada, & Lada (2001) also hold this opinion.

We inquire how the IC 5146 data bear upon this issue, even though L-band (3.5 μm) photometry is not available for IC 5146. Figure 9 is a display of our $J-H$, $H-K$ data for stars lying above the main sequence. For this purpose the Table 1 colors have been transformed to the CIT system via the relationships given by Carpenter et al. (1997): $(J-H)_{\rm CIT} = 0.953\ (J-H)_{\rm UKIRT}$ and $(H-K)_{\rm CIT} = 0.995\ (H-K)_{\rm UKIRT}$. The symbols are as in Figure 7. Also plotted are the intrinsic colors of main-sequence dwarfs and giants, and their limiting reddening lines. Those stars having Hα emission are indicated by crosses, the larger being CTTSs. Most CTTSs fall to the right of the rightmost reddening vector, while WTTSs tend to be confined within the reddening band.

To quantify this effect, we assume that most of the Hα emitters are likely to be K or M stars, which normally would lie along the leftmost edge of the reddening band in Figure 9. The $H-K$ excess $\Delta(H-K)$ is then the horizontal displacement from that line. In Figure 10 W(Hα) is plotted against $\Delta(H-K)$. The top dashed line is the WTTS-CTTS boun-

TABLE 4
WALKER VARIABLES

WALKER VAR.	TABLES 1 OR 2 (No.)	RANGE IN B	RANGE IN V	RANGE IN R	RANGE IN I	$W(\mathrm{H}\alpha)$	REMARK
1	497	16.38	15.63	15.28	14.10	50	LkHα 235
2[a]	525	21.36	19.86	18.43	16.51	170	
3[c]	...	...	...	...	...	<5	
4[c]	...	...	...	...	...	<5	
5	17	21.75–22.14	20.23–20.26	18.65–18.78	17.12–17.20	150	IHα 104
6[b]	...	21.64–21.66	20.20–20.27	19.32–19.34	18.39–18.39	...	
7[b]	...	21.41–21.37	19.86–19.93	18.94–18.94	17.99–17.99	...	
8	83	19.41–19.42	18.01–18.08	16.57–16.63	15.45–15.57	300	LkHα 242
9	116	19.21–19.35	17.72–17.79	16.59–16.63	15.17–15.33	46	LkHα 243
10[c]	...	...	...	...	...	<5	
11	190	18.80	20.38	16.90	15.47	60	IHα 132
12	197	22.31–22.69	20.39–20.67	18.98–19.15	17.54–17.75	24:	IHα 135
13	209	21.69–22.77	19.99–20.58	18.37–18.63	16.72–17.06	8:	IHα 137
14	228	22.50–22.69	20.36–20.39	18.77–18.81	16.49–16.58	6	IHα 143
15	234	19.63–20.06	17.76–18.31	16.55–17.04	15.11–15.65	4	IHα 146
16[b]	...	20.69–20.77	19.25–19.30	18.28–18.32	17.28–17.38	<5	
17	270	22.04–22.32	20.29–20.92	18.70–19.46	17.10–17.99	120:	IHα 159
18	291	17.80–18.27	18.00–18.27	16.82–16.95	15.56–15.71	16	LkHα 247
19	308	19.55–19.61	17.91–18.15	16.71–16.89	15.39–15.57	53	LkHα 248
20	326	18.83	17.06–17.15	15.87–15.92	14.76–14.84	160	LkHα 250
21	334	20.10–20.88	18.25–19.01	17.05–17.71	15.72–16.45	<5	

NOTE.—Single magnitudes from Table 1 or 2 are given for stars having observations at only one epoch.
[a] The star at the position marked for variable 2 on Walker's Fig. 2 has no detectable Hα emission and lies below the main sequence, so it is not included in Table 2. However, 525 = IHα 176 is about 5″ away, so we have assumed that it is Walker's variable.
[b] Lies below the main sequence, so is possibly a background star and not in Table 1 (or 2) for that reason.
[c] Outside the present photometric area.

dary, while the line below it marks the formal detectability limit of our grism system. Emission in most of the stars plotted below that line was detected with the CFHT MOS or slit spectrograms.

There is a general rise in $W(\mathrm{H}\alpha)$ to about $\Delta(H-K) = 0.45$, but with substantial scatter and what appears to be saturation thereafter. A similar plateau appears when $W(\mathrm{H}\alpha)$ is plotted against $K-L$ excess (Hartmann 1998, Fig. 6.9). There is no obvious discontinuity at the WTTS-CTTS boundary. Although $W(\mathrm{H}\alpha)$ does rise with IR excess in a statistical sense, it can hardly be considered a disk indicator in IC 5146: at any given $\Delta(H-K)$ there is a spread in $W(\mathrm{H}\alpha)$ by a factor of 10 or more. A similar result was found by Hughes et al. (1994) for TTSs in Lupus.

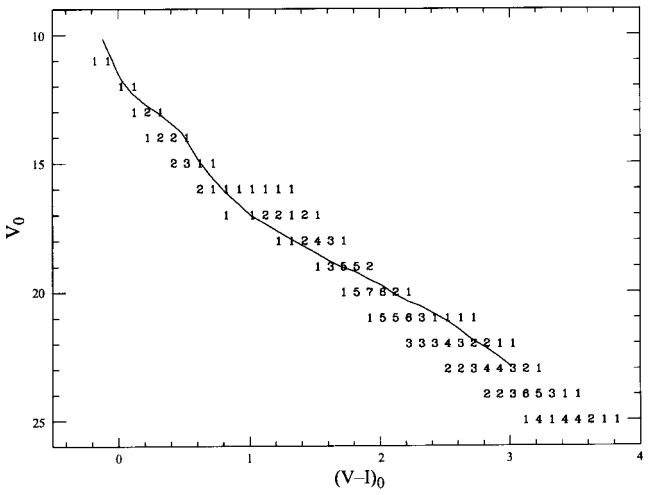

FIG. 8.—Predicted number of foreground stars projected onto a 7′ × 7′ area of IC 5146 and plotted in the color-magnitude plane as the number in each box of $\Delta V_0 = 1.0$ mag, $\Delta(V-I)_0 = 0.1$ mag. The distance cutoff is at 1.2 kpc (no background contribution is included), and it was assumed that the foreground A_V increases at a rate of 2.0 mag kpc^{-1}. All stars were dereddened for a mean extinction of $A_V = 3.0$ mag, for comparison with Fig. 7.

3.4. *Ages and Masses*

Pre–main-sequence evolutionary tracks have been computed for stars in the mass range of interest here by a number of workers; here we consider those published by or available from D'Antona & Mazzitelli (1997, hereafter DM97), Palla & Stahler (1999, hereafter PS99), Baraffe et al. (1998, hereafter B98), and Siess, Dufour, & Forestini (2000, hereafter S00). Each set of theoretical log L, log T_e coordinates was converted to the observational V_0, $(V-I)_0$ system by fitting to the *main-sequence* colors and bolometric corrections tabulated by Kenyon & Hartmann (1995). Then a dense mesh of isochrones, constructed by spline interpolation between points of equal age on each mass track, was entered for each star in Figure 7 to read off its age and mass. Figure 11 displays the results for each of the four theories as a histogram, where the open boxes represent all stars lying above the main sequence, and shaded boxes the Hα emitters.

Obviously the "age" of a star depends on when the clock was started. It is not obvious in every theory how $t = 0$ was defined, but its consequence can be seen by comparing the ages of a star of given mass at a common luminosity level near the beginning of each vertical track.

TABLE 5

NUMBER OF Hα EMITTERS DETECTED/NOT DETECTED, AND NUMBER OF FOREGROUND STARS EXPECTED IN IC 5146

	OBSERVED					FOREGROUND A_V (kpc^{-1})	
	Hα DETECTED						
$(V-I)_0$ INTERVAL CENTERED AT (1)	CTTSs (2)	WTTSs (3)	Hα Not Detected (4)	Too Faint (5)	Only Hα Emission (6)	1.0 (7)	2.0 (8)
0.50	0	0	4	2	0	1	3
0.80	2	1	13	1	0	5	4
1.10	5	3	28	11	0	16	10
1.40	7	2	35	20	1	15	18
1.70	8	4	9	19	1	6	16
2.00	7	3	15	25	2	2	9
2.30	10	3	7	10	1	4	3
2.60	1	1	7	14	0	3	5
2.90	7	0	5	16	2	3	7
3.20	0	0	3	16	0	2:	5:
3.50	1	0	1	4	1	...	...
3.80	1	0	0	1	0	...	...
4.10	0	0	0	1	0	...	...
4.40	0	0	0	0	0	...	...

NOTES.—Each line contains the number of stars detected in the grism survey, or expected, in the $(V-I)_0$ interval 0.3 mag wide centered on the value in col. (1). Col. (2): number having $W(\mathrm{H}\alpha) \geq 10$ Å. Col. (3): number having $W(\mathrm{H}\alpha) < 10$ Å. Col. (4): number whose continuum was above the threshold but for which no Hα emission was detected; a conservative upper limit of <5 Å was assigned in Table 1. Col. (5): number for which photometry was possible, but so faint that their continua were undetectable on the grism exposures. Col. (6): number for which only an Hα emission line was detectable above the sky background; these are labelled "em" in Table 1. Cols. (7), (8): number of foreground stars predicted (for two assumptions for the increase of A_V with distance) to lie above the Pleiades main-sequence line in Fig. 7, following allowance for the average A_V of 3.0 mag. Not included in these statistics: stars having $0 < W(\mathrm{H}\alpha) < 3$ Å detected on MOS spectrograms, because those observations were limited to brighter stars.

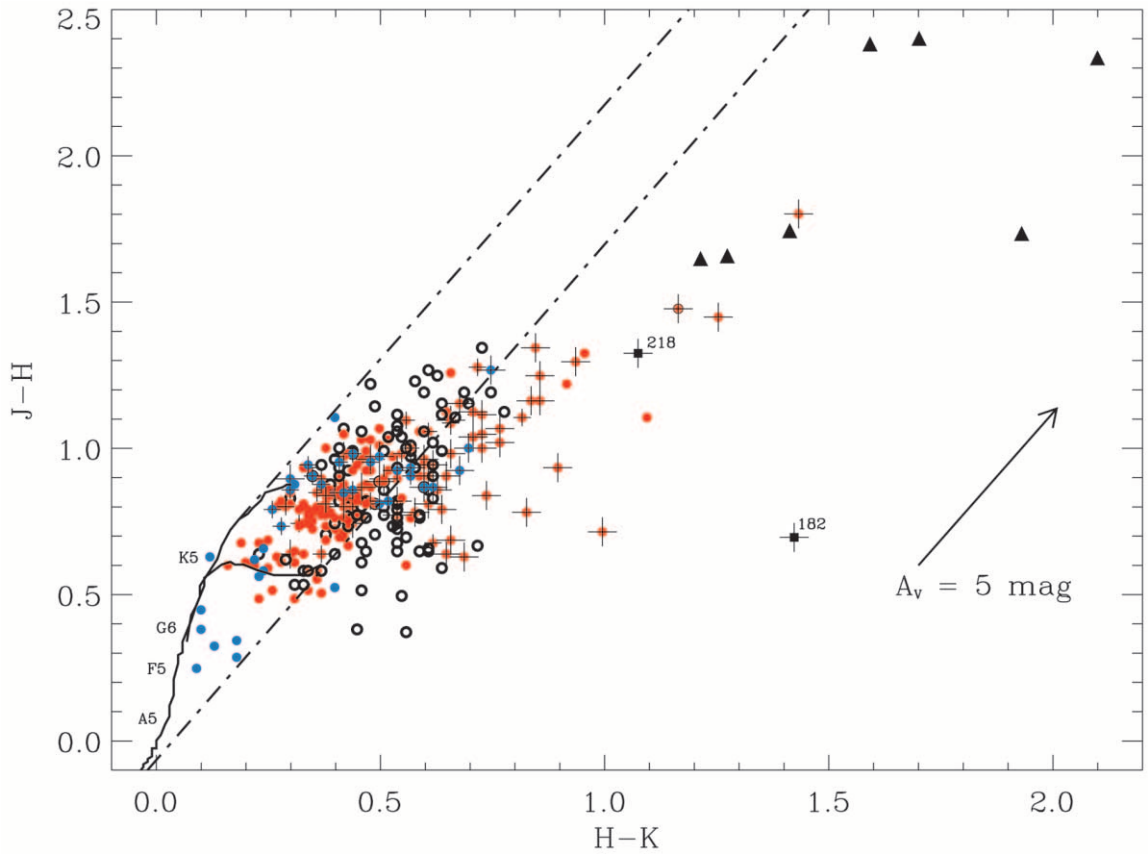

FIG. 9.—$J-H$ vs. $H-K$ data (from Table 1, converted to the CIT system as explained in the text) for the above–the–main-sequence stars of Table 1. Dashed curves mark the normal main-sequence and giant-branch loci, and dotted lines the strip across which normal stars would be translated by normal reddening. Symbols are as in Fig. 7, except the filled triangles, which represent the bright NIR sources in the southeast quadrant of IC 5146. The two filled squares correspond to the stars near +46°3474 having HH-like spectra (see § 3.7 and Fig. 13).

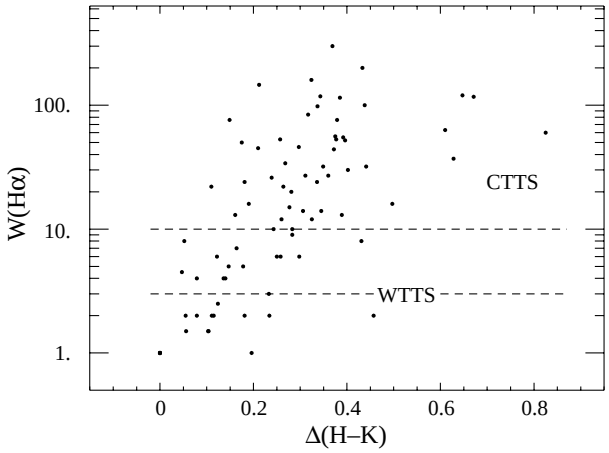

FIG. 10.—Log $W(\mathrm{H}\alpha)$ vs. the $H-K$ excess (estimated as explained in the text) for those stars of Fig. 9 having Hα in emission. The dashed lines mark the domains of CTTSs (*above*), WTTSs of 3 Å $\leq W(\mathrm{H}\alpha) \leq$ 10 Å detected on grism spectrograms (*between the lines*), and stars having $W(\mathrm{H}\alpha) < 3$ Å, detected mainly on the MOS spectrograms (*below*).

Table 6 contains samples of log ages from each theory. The luminosities chosen were high enough to intercept all the tabulated tracks but conditioned by the fact that the B98 tracks begin at 1 Myr. One sees that the age offsets with respect to the initial B98 log age of 6.0 are mostly positive; i.e., ages near the beginning of the other tracks tend to be older than the B98 values. But because the offsets are mass dependent and because differences in the theories become manifest as time goes on, the age profiles of Figure 11 differ from one another in both shape and position along the age axis.

This effect is apparent in the last columns of Table 6, which give the median ages from each theory for the Hα emitters and for all stars above the main sequence.

3.5. *The* Hα*-Emission Stars: Distribution, Statistics*

The equivalent width of Hα emission is an index of the level of stellar or circumstellar activity, but not in a physically well-defined sense since it is relative to the stellar continuum at that wavelength.[3] Nevertheless, $W(\mathrm{H}\alpha)$ is a readily measurable quantity in stars for which little else may be known. Single stars on the main sequence having Hα equivalent widths in the CTTS range are rare, which must mean that CTTS Hα strengths diminish as those stars become older. So, if *all* stars are CTTSs when they first become optically detectable, then WTTSs ought on the average be older than the CTTSs. This is known not to be the case in IC 348 (Herbig 1998) or in Taurus (Hartmann 2001).

Figure 12 shows the situation in IC 5146 as a plot of $W(\mathrm{H}\alpha)$ versus log age according to DM97; filled circles are stars of known spectral type. The ages of stars of unknown type (*open circles*) depend on the assumption that the mean cluster $A_V = 3.0$ mag applies. If their spectral type had been known, that point would have moved to a lesser age for later

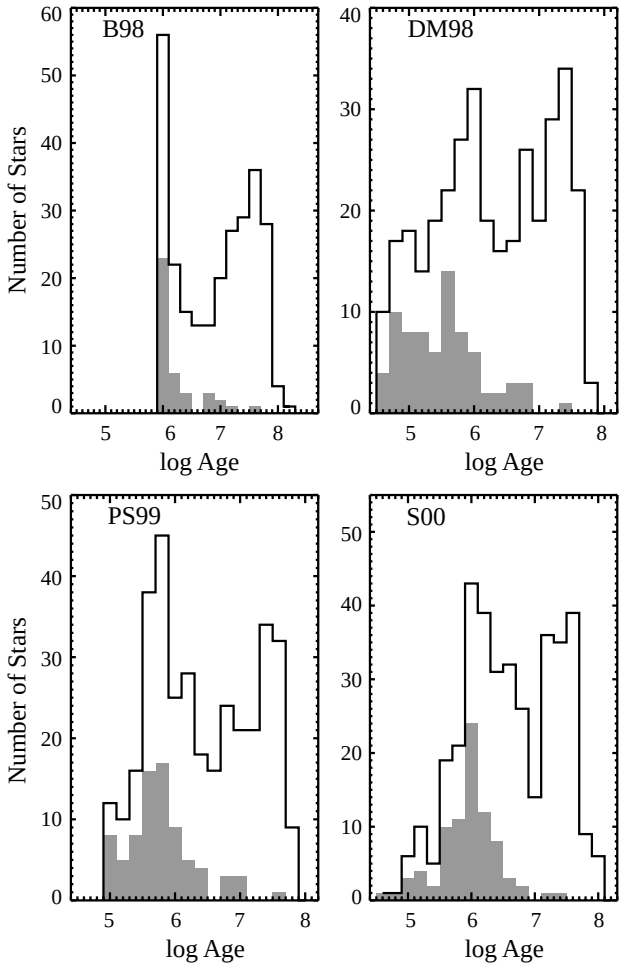

FIG. 11.—Histograms showing the distribution of ages of stars above the main sequence in IC 5146, as estimated from their location in the V_0, $(V-I)_0$ diagram of Fig. 7, and isochrones obtained from the sources indicated in each panel. The shaded segments represent Hα emitters alone, likely members of IC 5146. The open sections represent all others, certainly including a large number of foreground nonmembers.

types or to a greater age for earlier ones. The horizontal bars on several points show typical age excursions corresponding to types ranging from G0 V to M0 V. Given such uncertainty, the open circles are of low weight. If only the filled circles are considered, then a formal application of Spearman rank correlation and Kolmogorov-Smirnov tests would indicate that there is a significant inverse correlation of log $W(\mathrm{H}\alpha)$ and log age at the 95%–98% confidence level. However, we do not take this seriously: it depends crucially on the very few points having log age > 6.5 and on how much confidence one has in ages obtained from present-day theoretical tracks. In other words, we see no persuasive evidence that the WTTSs in the IC 5146 are older than the CTTSs.

It would be prudent to keep in mind the possibility that WTTSs may *not* begin as CTTSs: they may first become optically detectable at that lower level of Hα emission.

Additional statistics for IC 5146 are shown in Table 7, which gives the numbers of Hα emitters per square parsec boxed by $W(\mathrm{H}\alpha)$ and M_V. The table extends beyond the observational cutoff at about $M_V = +7.6$, which is based on a Hα detection limit at $V \approx 21.0$ and a distance of 1.2 kpc

[3] A better index would be $L(\mathrm{H}\alpha)/L_{\mathrm{bol}}$, which can be estimated given reddening-corrected *VRI* magnitudes and the appropriate bolometric correction. For example, if $W(\mathrm{H}\alpha) = 10$ Å, then $L(\mathrm{H}\alpha)/L_{\mathrm{bol}}$ is 1.4(−3) for a normal G0 V, 1.3(−3) at K5 V, and 0.6(−3) at M3 V, where $A(B)$ is an abbreviation for $A \times 10^B$.

TABLE 6
AGES FROM DIFFERENT THEORIES

$M/M_\odot$:	1.0	0.6	0.4	0.1		
log $L/L_\odot$:	0.13	−0.17	−0.39	−1.16	Only Hα Emitters	All above Main Sequence
(1)	(2)	(3)	(4)	(5)	(6)	(7)
Baraffe et al. 1998	6.00	6.00	6.00	6.01	<6.18	<7.20
D'Antona & Mazzitelli 1997	6.30	6.15	6.04	6.05	5.57	6.35
Palla & Stahler 1999	6.27	6.25	6.23	6.18	5.87	6.40
Siess et al. 2000	6.29	6.26	6.25	6.54	6.18	6.70

NOTES.—Cols. (2)–(5) show the effect of the different zero points of the age coordinate implicit in the several theories. The numbers are the log ages (in years) interpolated at a common log $L/L_\odot$ level in tracks for four different masses. Cols. (6) and (7) give the median (log) ages for the emission-Hα stars and for all above–the–main-sequence stars for the same theories. The Baraffe et al. values are too large because no tracks for ages < 1 Myr were available, and hence younger stars are not represented in those medians.

and assumes that all stars lacking a spectral classification have the average extinction of $A_V = 3.0$ mag. For comparison, Table 7 also contains the same data for IC 348, the only other cluster for which similarly homogeneous data are currently available. They apply only to the central photometric region of IC 348 (Herbig 1998, Table 1) for which the observational cutoff is at about $M_V = +10.7$. Hα detections below these levels probably correspond to stars having lower than average A_V values.

A comparison of the two clusters shows that (1) the surface density of Hα emitters brighter than $M_V = +7.6$ is higher in IC 348 than in IC 5146 by a factor of 2.5; (2) the fraction of Hα emitters that are WTTSs is 0.52 ± 0.12 for IC 348 and 0.23 ± 0.06 for IC 5146 (i.e., the proportion of WTTSs is significantly higher in IC 348[4]); (3) it is uncertain whether the number of Hα emitters peaks in the $M_V = +6$ to +9 range or continues to rise to fainter magnitudes.

3.6. *Other Interesting Stars*

W46 and W66 both illuminate small reflection nebulae, so obviously they lie in the volume occupied by the cluster. From their location in Figure 7, they appear to be fairly massive ($\approx 2.5\ M_\odot$) pre–main-sequence members of IC 5146. W46 (= LkHα 245) is type K0, has fairly strong Hα emission (W = 28 Å), a small $H-K$ excess, and shows on an MOS spectrogram strong absorption at 6707 Å that is probably the Li I line. W66 lies nearer the main sequence on the same 2.5 $M_\odot$ track. It is type F0, has a central emission spike ($W = 1.7$ Å) in its Hα absorption line, but, on the basis of Elias's photometry, has little if any $H-K$ excess.

These two interesting pre–main-sequence stars deserve a closer examination. Unfortunately, we were unable to obtain high-resolution spectra of either, or of any of the others that lie near W46 in the color-magnitude diagram.

[4] A similar difference between the TTS populations of Ori OB 1a and Ori OB 1b has been noted by Briceño et al. (2001).

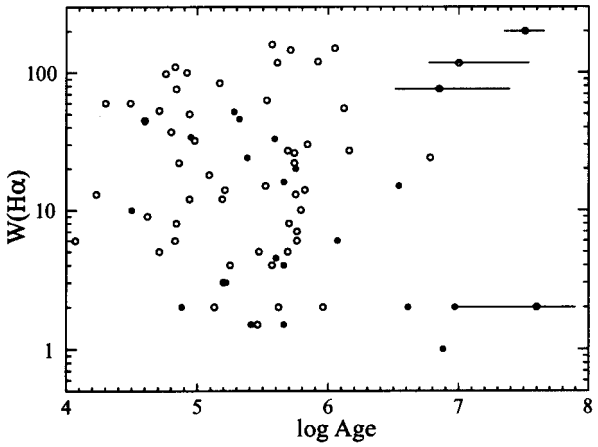

FIG. 12.—Dependence of log W(Hα) on age in IC 5146. Filled circles represent stars of known spectral type, open circles those of unknown type, plotted under the assumption that their reddening is that of the cluster mean. The horizontal lines through several such points show how far that point would move if the type were really M0 V (*to the left*) or G0 V (*to the right*).

3.7. *HH Objects*

There are two stars near BD +46°3474 that were suspected to be HH objects because on the grism spectrograms a second emission line was present longward of Hα, at about the position expected for [S II] $\lambda\lambda$6716, 6730. These stars, both about $R = 19$, are entries 182 (= IHα-130) and 218 (= IHα-141) in Table 1. They are located 16″ and 21″, respectively, from BD +46°3474; the second is clearly diffuse on the R-band images, with a short tail extending about 1″ northward (see Fig. 13). Both have large $H-K$ excesses; they are marked as filled boxes in Figure 9.

John Tonry very kindly obtained spectra of both stars for us on 2000 November 28 with the ESI (Echellette Spectrograph and Imager on the Keck II telescope; at Hα its dispersion is 24 km s^{-1} per 15 μm pixel). These spectra extend from about 0.5 to 1.09 μm and show many emission lines on weak continua.

They indeed have spectra resembling HH objects, but with a strong stellar component. There appear to be two separate contributors to the emission spectrum of object 218: the many forbidden lines of [C I], [N II, [O I], [O II], [S II], [S III] are characteristic of HH objects, while the Ca II IR triplet lines and O I λ8446 are as strong as in some TTSs. Presumably the continuous spectrum is contributed by that component. An unusual feature is the presence of weak lines of N I (RMT 1, 2, and 3) in both sources. The Hα line of the grism spectra is now seen to contain a substantial contribution from [N II] $\lambda\lambda$6548, 6583. The H lines (Hα and P7 through P19) are probably common to both contributors. The spectrum was extracted in a narrow strip 1.″7 wide centered on the continuum. In this sample, all unblended lines have about the same radial velocity; the average of 33 H and forbidden lines is -2 ± 1 km s^{-1}.

TABLE 7
STATISTICS OF $W(H\alpha)$ VERSUS M_V IN IC 5146 AND IC 348

	$W(H\alpha)$						
M_V	3–9 Å	10–29 Å	30–49 Å	50–69 Å	70–89 Å	> 90 Å	N
			IC 5146				
+1.0	...	...	...	...	...	...	2
+2.0	0.2	...	0.2	...	...	...	2
+3.0	0.4	0.2	...	...	...	...	3
+4.0	0.2	0.2	0.4	...	...	0.4	13
+5.0	1.0	0.8	0.8	0.4	...	0.2	12
+6.0	0.8	0.6	...	0.2	0.2	0.4	22
+7.0	0.8	1.7	0.2	0.2	0.2	1.5	9
+8.0	...	0.4	...	...	0.2	0.6	6
+9.0	...	0.2	0.2	0.4	...	0.6	4
+10.0 ..	...	...	...	...	...	...	...
+11.0 ..	...	...	...	...	...	...	...
+12.0 ..	...	...	...	...	...	...	...
N	17	20	9	6	3	18	...
			IC 348				
+1.0	...	...	...	...	...	...	...
+2.0	...	...	...	...	...	...	...
+3.0	...	1	...	...	...	...	1
+4.0	...	...	...	...	...	...	...
+5.0	1	...	...	...	...	...	1
+6.0	3	...	1	1	...	1	6
+7.0	10	3	3	1	1	...	18
+8.0	8	1	3	1	...	1	14
+9.0	5	2	2	2	...	...	11
+10.0 ..	2	3	2	...	...	...	7
+11.0 ..	3	...	...	...	...	...	3
+12.0 ..	...	...	...	...	...	...	...
N	32	10	11	5	1	2	...

NOTES.—The entries are the number of stars per square parsec in that $M_V \pm 0.5$ mag, $W(H\alpha)$ box. The distance assumed for IC 5146 is 1.2 kpc and a search area of 4.8 pc^2; those same quantities for IC 348 are 320 pc and 1.05 pc^2. The Ns are the actual number of stars in that row or column. The dotted lines mark the approximate detection limit for Hα emission for each cluster.

The slit was set in P.A. 144° for object 218 and thus partially sampled the wisp extending northward. The Hα, [S II], and [N II] lines extend along the slit on both sides of the continuum, and they show large velocity shifts of the opposite sign on the two sides. Out to about 1.″5 to the southeast the velocity peaks at about +200 km s^{-1}, and out to 2.″2 to the northwest at about −200 km s^{-1}.

The spectrum of 182 contains many of the same emission lines, both permitted and forbidden, but differs in that the Ca II lines $\lambda\lambda$8498, 8542, 8662 are not present, unlike 218 where they dominate the blending Paschen lines P16, P15, and P13. The continuum also is much fainter than in 218. The mean velocity from 36 emission lines is +2 ± 1 km s^{-1}. Note that these velocities are purely nominal and should be treated with caution; there was no external check on the velocity system. The spectra of both sources in the 8000–9200 Å region are plotted in Figure 14.

The R brightnesses of both objects are inflated significantly by the contribution of the emission lines in that passband: in 182 the equivalent width of Hα alone is 1100 Å, and in 218 it is 350 Å. If the reference continuum has the energy distribution of a K5–M0 dwarf, then the observed R values are too bright by 0.49 and 0.18 mag, respectively.

We have no explanation for the fact that the only such objects in IC 5146 lie very near the central star. There are no IR sources on the K-band images on the line connecting 182 and 218 that might account for them as products of an outflow.

3.8. *The Spectrum of BD +46°3474*

BD +46°3474 (= W42) is type B1 V (Morgan, unpublished, quoted by Walker 1959) or B0 V (Crampton & Fisher 1974). We adopt the latter type in what follows, because the ratio of He II λ4685 to He I λ4711 in +46°3474, when compared with the standards reproduced in the digital atlas of OB spectra of Walborn & Fitzpatrick (1990), shows that B0 V is the better match. B0–B1 is near the transition point on the main sequence where H ionization of a surrounding cloud has diminished to the point that dust scattering predominates, thus accounting for the mixed classification of the IC 5146 nebulosity.

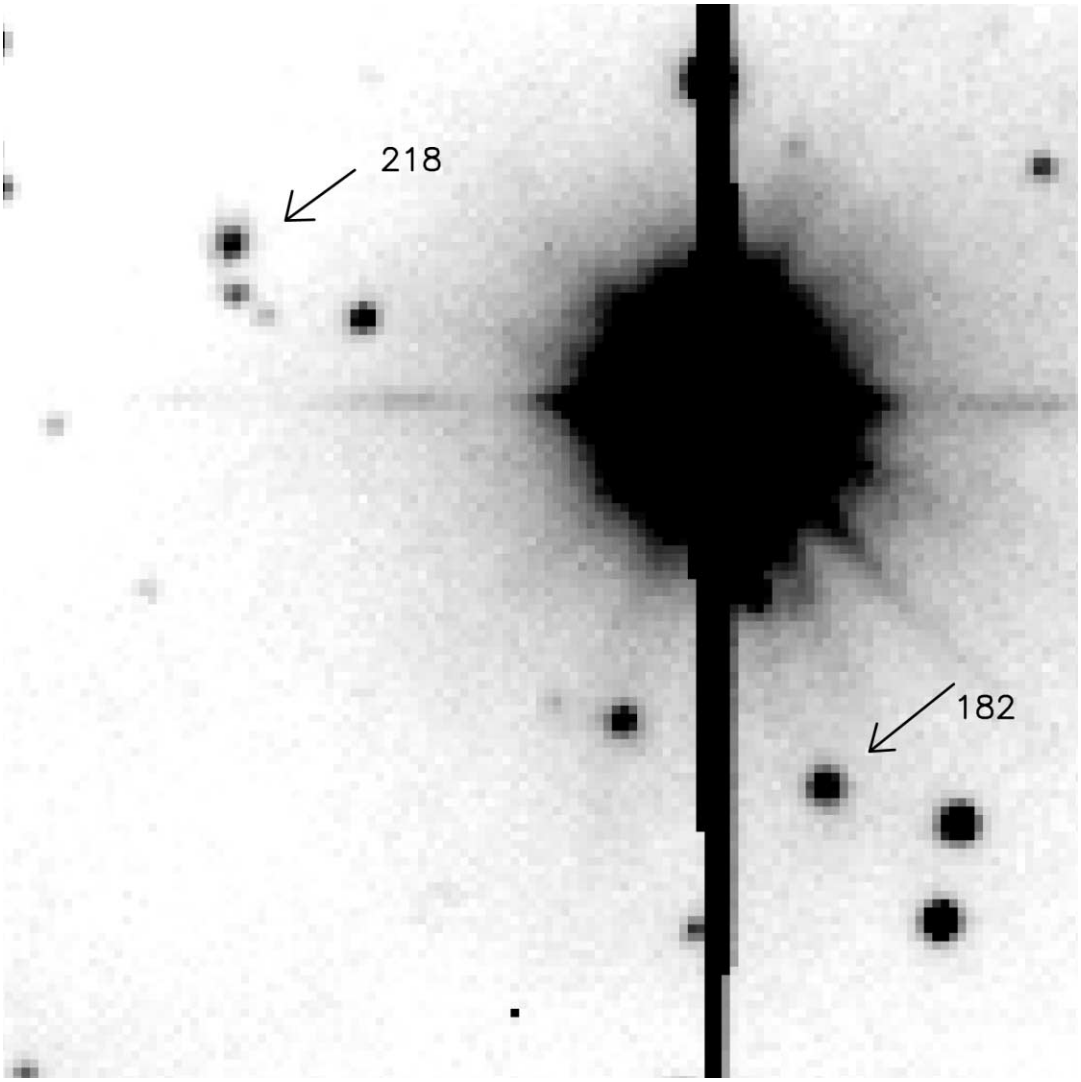

FIG. 13.—Immediate vicinity of BD +46°3474 (the very bright star), with the two stars having HH object–like spectra identified. The field shown is about 44″ on a side; north is at the top, and east to the left.

The star is a close binary, discovered by Couteau (1987) and measured visually in 1985.75 at 185°.1, 0″.92, 9.7–11.8 mag. The duplicity is evident on our short-exposure CCD images, but photometry is difficult because the primary is always saturated.

Despite the likelihood that +46°3474 is even younger than the low-mass pre–main-sequence population of the surrounding cluster, there is no sign at HIRES resolution of any of the spectral abnormalities one associates with HAeBe stars: there is no emission in Hα or Hβ, nor any sign of P Cyg structure at those lines or elsewhere in the 4300–6700 Å region. The only unusual feature is the remarkable narrowness of the absorption lines as observed at a resolution of 45,000. As a consequence the radial velocity can be measured with some confidence; it was -4.8 ± 0.2 km s^{-1} on the HIRES exposure of 2000 February 2 and -4.9 ± 0.2 km s^{-1} on 2000 November 5. The four low-resolution velocities published by Liu, Janes, & Bania (1989, 1991) average -5 ± 1.5 km s^{-1}, so there is no indication that the velocity is not constant.

The intrinsic widths of five weak unblended O II and C II lines were measured by fitting Gaussians to the 2000 February 2 profiles and removing quadratically the instrumental contribution by similar fits to thorium lines and the thermal Doppler width for an assumed temperature of 33,000 K. The resultants, assumed to represent pure rotational broadening, correspond to $v \sin i = 10$ km s^{-1}, a small value for an early B-type star but not without precedent (Kilian 1992; Gies & Lambert 1992).

The interstellar Ca II lines in +46°3474 are clearly double, with a suggestion of a third component. Their profile can be reproduced by a composite of three overlapping lines of adjustable position, strength, and width. The variation of optical thickness across each was taken to be Gaussian, and the line depth simply exp $(-\tau_\lambda)$ at each point. Figure 15 shows the best fit to Ca II λ3968. The crosses represent the data points, the dotted contours outline the individual components, and the solid line shows their sum. The resulting parameters for both Ca II lines (λ3933 was measurable in two orders) are given in Table 8. The interstellar Na I lines

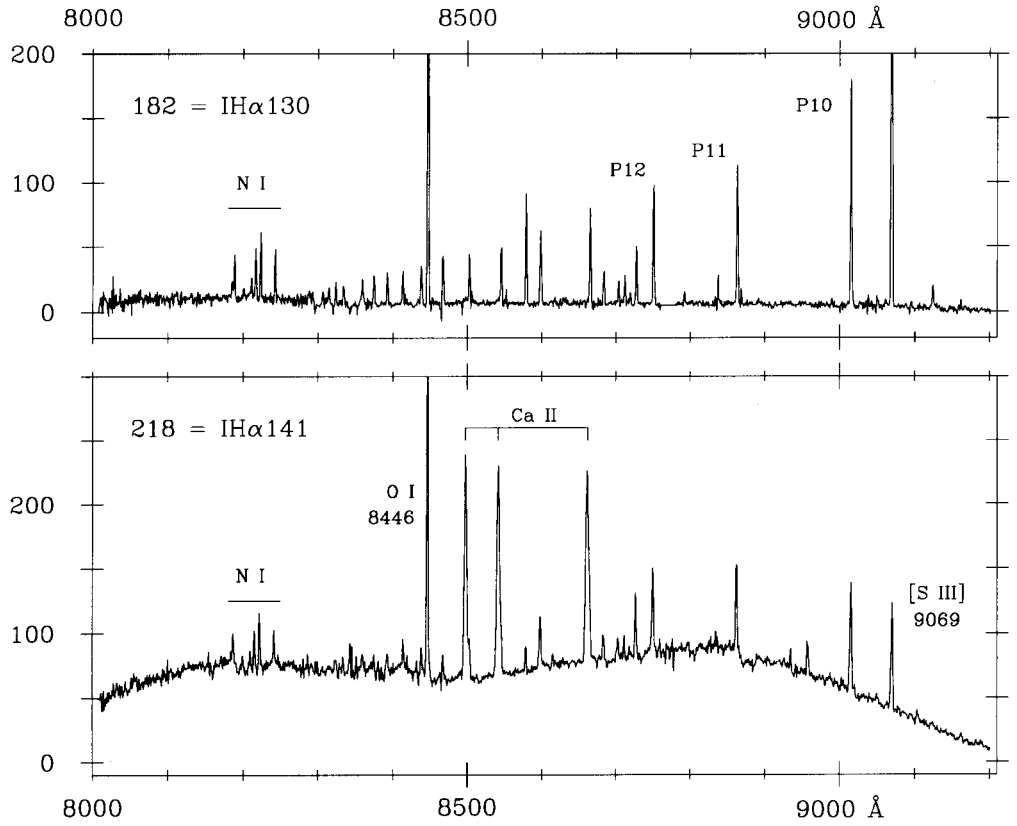

FIG. 14.—Spectra of objects 182 and 218 between 8000 and 9200 Å, illustrating the striking difference between the two sources. In IHα 141 (*bottom*) the continuous spectrum and the IR Ca II triplet are strong, while both are weak or absent in IHα 130 (*top*). The strong O I 8446 Å line is off scale on both. An absorption band near 8860 Å in IHα 141 may be due to TiO. Both spectra were divided by a continuum source, so the blaze function has been removed, but there has been no allowance for atmospheric or interstellar extinction, so the fluxes are on an instrumental system. A number of weak emission lines that coincide with sky or H II features have been blanked out in cases where the background subtraction is suspect.

at 5889, 5895 Å are much stronger, but the same three components can be recovered from those heavily saturated profiles, although with greater uncertainties. The Na I structure and velocities and equivalent widths for several (single) interstellar lines of CH, CH^+, and CN are also given in Table 8.

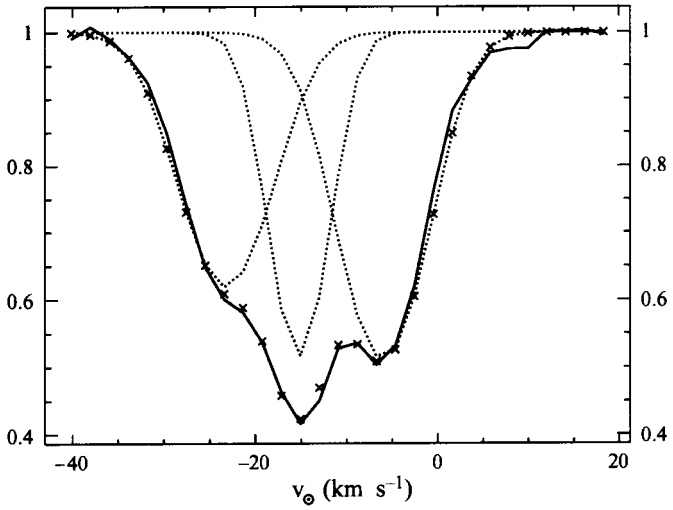

FIG. 15.—Profile of the interstellar Ca II λ3968 line in BD +46°3474. The solid line connects the data points, the dotted contours show the profiles of the 3 components into which the line was decomposed, and the crosses outline the profile reconstructed as their sum, i.e., the fit to the observations.

It is of interest to compare this interstellar structure, with separate components at −6, −15, and −22 km s^{-1}, with those measured for other distant stars in the same direction. Adams (1949) gives interstellar (IS) *K*-line velocities for four stars within 6° of IC 5146. In those bright OB stars the IS lines are single, with a mean velocity of −14 km s^{-1} (after allowance for the modern value of the laboratory wavelength of the *K* line). Münch (1957) published *K*-line velocities for four additional, much fainter, OB stars in the same region. In all of these, the main IS component is at −14 km s^{-1}, while in three there is an additional component at −40 km s^{-1}. The −14 km s^{-1} feature is formed in the Orion arm, foreground to all these stars and to +46°3474, where it is also present at −15 km s^{-1}. The −40 km s^{-1} component seen in Münch's stars is formed in the distant Perseus arm at 2–3 kpc, so its absence in the much nearer +46°3474 is understandable.

Neither the −6 or the −22 km s^{-1} IS line in +46°3474 has a counterpart in any of these stars, so they are apparently local to IC 5146. The interstellar Ca II lines in BD +46°3471, only 10′ away, are strong and single at −10 km s^{-1}, with no indication of a component near −22 km s^{-1}, although a contributor at −6 km s^{-1} could be concealed in the blend. The −6 and −22 km s^{-1} clouds may be related to the kinematics of IC 5146 discussed in § 3.9.

The IS lines in +46°3471 were measured as single also by Catala et al. (1986). They found the Ca II λ3933 line at −10.8 km s^{-1} (at a resolution of about 30,000), the Na I lines at −11.1 km s^{-1}, and Mg II λ 2795 at −16 km s^{-1}.

TABLE 8
PARAMETERS OF THE INTERSTELLAR LINES IN BD +46°3474

Ion	λ	Component	Central $v_{\odot}$	Central τ	σ (mÅ)	W (mÅ)	Total W (mÅ)
Ca II	3933.664	1	−5.5	1.30	58.	125.	277.
		2	−14.2	1.30	40.	87.	
		3	−22.5	0.94	60.	105.	
Ca II	3968.470	1	−6.0	0.67	60.	81.	184.
		2	−15.2	0.66	40.	53.	
		3	−23.2	0.48	63.	64.	
Na I.....	5889.953	1	−6.6	3.5	130.	464.	668.
		2	−15.1	1.0:	80.:	145.:	
		3	−19.8	4.0	95.	355.	
Na I.....	5895.923	1	−7.6	3.4	120.	423.	587.
		2	−15.1	0.5:	80.:	85.:	
		3	−21.1	2.6	75.	237.	
CH^+ ...	4232.548	...	−7.3	...	...	...	38.
CH^+ ...	3957.692	...	−7.4	...	...	...	23.
CH^+ ...	3745.31	...	−7.6	...	...	...	10.
CH.....	4300.313	...	−7.6	...	...	...	22.
CN.....	3874.608	...	−7.6	...	...	...	17.

Something more can be inferred from the strengths of the diffuse interstellar band (DIB) spectrum, which is fairly strong in both +46°3474 and +46°3471. Some bands are well-enough defined to serve as a rough check on the velocities from the atomic lines, although their diffuseness would smear out any individual cloud structure. DIB rest wavelengths have been determined by several investigators from the displacements of atomic and molecular lines in reddened OB stars. With the rest wavelengths given by Herbig (1995), the mean DIB velocity in +46°3474 is -9 ± 1 km s^{-1} and is -12 ± 2 in +46°3471. The wavelengths tabulated by O'Tuairisg et al. (2000) would give -11 ± 1 and -14 ± 2 km s^{-1}, respectively. There is thus no indication that the DIBs do not share the motion of the foreground Ca II and Na I clouds.

However, the equivalent widths of some of the same DIBs given in Table 9 [together with the $E(B-V)$ values of the two stars] show that the DIB strengths are nearly the same in both, despite the color excess of +46°3474 being over twice as large. This latter rests on the assumption that the intrinsic color of +46°3471 is that of type A0 III, following Gray & Corbally (1998). This DIB discrepancy would be explained if the star is in fact much bluer, which, given its peculiar emission-line spectrum (see § 4.3) would not be surprising.

TABLE 9
EQUIVALENT WIDTHS OF DIFFUSE BANDS

Star:	+46°3474	+46°3471
$E(B-V)$ (mag):	1.08	0.45
λ (Å)	(mÅ)	(mÅ)
5797	80.	84.
5849	27.	24.
6203	60.	46.
6269	41.	28.
6379	28.	25.
6613	110.	86.
6699	7.	7.

3.8.1. *The Structure of IC 5146: Embedded Sources*

The nebulosity illuminated by BD +46° 3474 is approximately central in the larger molecular cloud seen optically in silhouette against the background star field. Far-infrared (Sargent et al. 1981; Wilking, Harvey, & Joy 1984) and CO (Lada & Elmegreen 1979; McCutcheon, Roger, & Dickman 1982; Dobashi et al. 1992) maps show a minimum near the center, such that at those wavelengths the appearance is of a broken ring around the bright nebula with maxima about 5′ north, 5′ southeast, and 5′–7′ west of +46°3474. On the other hand, the 21 cm line and continuum emission appear symmetrically distributed around the central star (Israel 1977; Roger & Irwin 1982).

Lada & Elmegreen (1979), Sargent et al. (1981), and McCutcheon et al. (1982) speculated that the southeast CO/FIR peak might be powered by an embedded hot star. However, the 2 and 10 μm survey of the area by Wilking et al. (1984) found only one infrared source, at $K = 12.8$. From their inference that late B was the earliest possible spectral type for this object, Wilking et al. concluded that, even if embedded in the cloud, it would be energetically incapable of explaining the observed CO and dust temperatures.

Forte & Orsatti (1984) found another very red star, our 312 (saturated on our shortest NIR exposures, but estimated to be about $K = 7.0$), south of IC 5146; it is plotted at (17.28, 3.59) in Figure 7. The star has no detectable Hα emission. It was suspected of variability on the strength of a V difference of 0.2 mag between our two epochs. The entry in Table 1 (the mean of those two observations) is 0.45 mag fainter in V and 0.35 mag redder in $V-I$ than measured by Forte & Orsatti, although those differences are in the sense of the systematic offsets between the two photometric systems (Fig. 4) and so may not be real. The short-exposure K-band images show 312 to be multiple, with a faint companion 2″.5 southeast and another 4″.0 northeast. As Forte & Orsatti pointed out, it could be either a background K- or M-type giant or a heavily reddened early-type cluster member. A Mauna Kea spectrum of the 2 μm region obtained in

TABLE 10
SOUTHEAST QUADRANT BRIGHT NIR SOURCES

Star	α	δ	J	$J-H$	$H-K$
IR-1	21 53 32.45	47 14 22.9	17.61	2.50	1.60
IR-2	21 53 33.20	47 14 18.9	17.97	2.45	2.11
IR-3	21 53 35.91	47 12 12.2	15.01	1.74	1.28
IR-4	21 53 41.98	47 14 27.1	17.57	1.82	1.94
IR-5	21 53 46.84	47 13 23.0	18.47	1.83	1.42
IR-6	21 53 49.71	47 13 52.6	18.27	2.52	1.71
IR-7[a]	21 52 37.87	47 14 37.9	16.52	2.34	1.62
WHJ-IR1 ...	21 53 50.65	47 13 22.5	15.46	1.73	1.22

NOTE.—Units of right ascension are hours, minutes, and seconds, and units of declination are degrees, arcminutes, and arcseconds (J2000.0).
[a] IR-7 is near BD +46°3471, not in the southeast quadrant.

2001 shows strong CO bands in absorption, so 312 is a late-type giant.

The reddest star found by Forte & Orsatti is our 239, at (19.02, 3.11) in Figure 7. It lies slightly to the right of the reddening band in $J-H$, $H-K$ (Fig. 9) but is too faint to determine whether Hα is in emission. It could well be a low-mass cluster member.

To discover whether still fainter sources exist within the southeast CO/FIR peak, the area was more thoroughly surveyed in J, H, and K with QUIRC in 2000 November. The field center was chosen to include Wilking et al.'s IR source, as well as 312 of Table 1.[5] Seven additional bright NIR sources were found, including Wilking et al.'s IR-1, which is probably the *IRAS* point source 21519+4659; it lies just outside the boundary of the optical survey. Table 10 gives the coordinates, J magnitudes, $J-H$, and $H-K$ colors of these seven objects. Only IR-4 was optically detected, in I. IR-2, which may be the *IRAS* point source 21516+4700, is attached to a faint arclike structure extending about 5″ to the northeast. IR-3, which falls outside the optical region, is located just west of 312. At $K = 12$, it is the brightest of the objects in Table 10. IR-5 lies within a bright arc of nebulosity together with several other faint red stars. Numerous other NIR sources lie within the boundaries defined by W53, W70, W66, and W76. It is apparent from stellar number densities in the optical that this southeast quadrant is significantly more opaque than the central region of the cluster.

Since no early B-type star has been found in this region, we concur with the conclusion of Wilking et al. that +46°3474 is the most massive and hence energetic member of IC 5146. The objects of Table 10 may represent intermediate-mass class I or II IR sources lying along the edges of the remaining molecular cloud. It is possible that protostellar outflows from stars forming in the region supplement the energy of the molecular cloud.

3.8.2. *The Structure of IC 5146: The Dark Lanes*

The appearance of IC 5146—a bright, approximately circular nebulosity with an early-type central star crossed by several dark lanes—is reminiscent of the Trifid Nebula, NGC 6514, excited by an O7 V star. The bright edges on some of those lanes have been explained (Lynds & O'Neil 1985) as ionized rims on dark clouds embedded in the H II region. More recently, a similar scenario has been invoked by White et al. (1999) in their discussion of the elephant trunk structures in NGC 6611. If the analogy otherwise holds for IC 5146, ionized edges would not be expected on account of its cooler central star, and indeed none are seen.

If the segmented structure of IC 5146 is caused by dusty clouds in front of the bright nebulosity, then the contrast between lanes and background should be wavelength dependent, which is susceptible to test as follows.

The straight lines in the R-band image of Figure 16 represent 5 pixel–wide slices across several of the dark lanes. Surface brightnesses along these cuts were extracted in $BVRI$. The brightness of the nebular background behind the cloud was inferred by interpolation between the ends of each slice, while the background upon which the nebula itself is projected was obtained by sampling around the edge of the bright nebulosity. The most opaque section of each slice is marked by short lines in Figure 16, and the mean extinction in that segment in magnitudes, together with its 1 σ uncertainty, is given in Table 11. Those A_λ values (with respect to the background) are plotted against λ^{-1} in Figure 17, together with the corresponding values at those wavelengths for normal interstellar extinction. The A_R's of these clouds in IC 5146, ranging between 0.8 and 1.3 mag, are somewhat less than the 1.5 mag quoted by Lynds & O'Neil (1985) for a dust lane in NGC 6514.

Table 11 also lists for each of the four clouds the value of $R_V = A_V/A_B - A_V$ that follows. Not included in the tabulated uncertainties is the effect of systematic error in the background sampling. Nevertheless, the slope of extinction versus wavelength is sufficiently similar to that expected for interstellar reddening to support the foreground cloud interpretation, although the errors are such that normality of the reddening law (i.e., that R_V is about 3.1) is not demonstrated. It is demonstrated, however, that the dark lanes are foreground clouds and not simply gaps in the bright nebulosity.

But if these clouds were in the *far* foreground of the cluster, one would expect a correlation between the A_V values of individual stars and the local surface brightness of the nebulosity. No such correlation is observed: that is, the stars projected upon dark lanes are no more likely to have large A_V values than do those on bright nebulosity. Similarly, there is no indication that stars having Hα in emission tend systematically to avoid dark lanes. Since most of those stars are certainly cluster members, it follows that the dark clouds lie within the star-forming volume, not in the far foreground. We therefore regard them as fragments of the front surface of the original molecular cloud that have survived the opening of a blister (Israel 1978) by BD +46°3474.

3.9. *The Kinematics and History of IC 5146*

Our picture of IC 5146 is very similar to that noted by Lada & Elmegreen (1979) and elaborated by Roger & Irwin (1982), namely, that BD +46°3474 formed fairly recently (the latter estimated 10^5 yr ago) in what is now the near side of a dense molecular cloud. It then ionized and dissociated the nearby H and CO and formed a blister on the cloud surface from which the hot gas is now being expelled. This is reminiscent of the champagne outflow envisaged, for exam-

[5] The bright K-band source found by Elias (1978), marked on his Fig. 1*b* lies outside the region surveyed, about 4.′5 southeast of our field center. Judging from the 2MASS three-color image of the field, it is likely that Elias's source is W74; no other bright NIR sources are nearby.

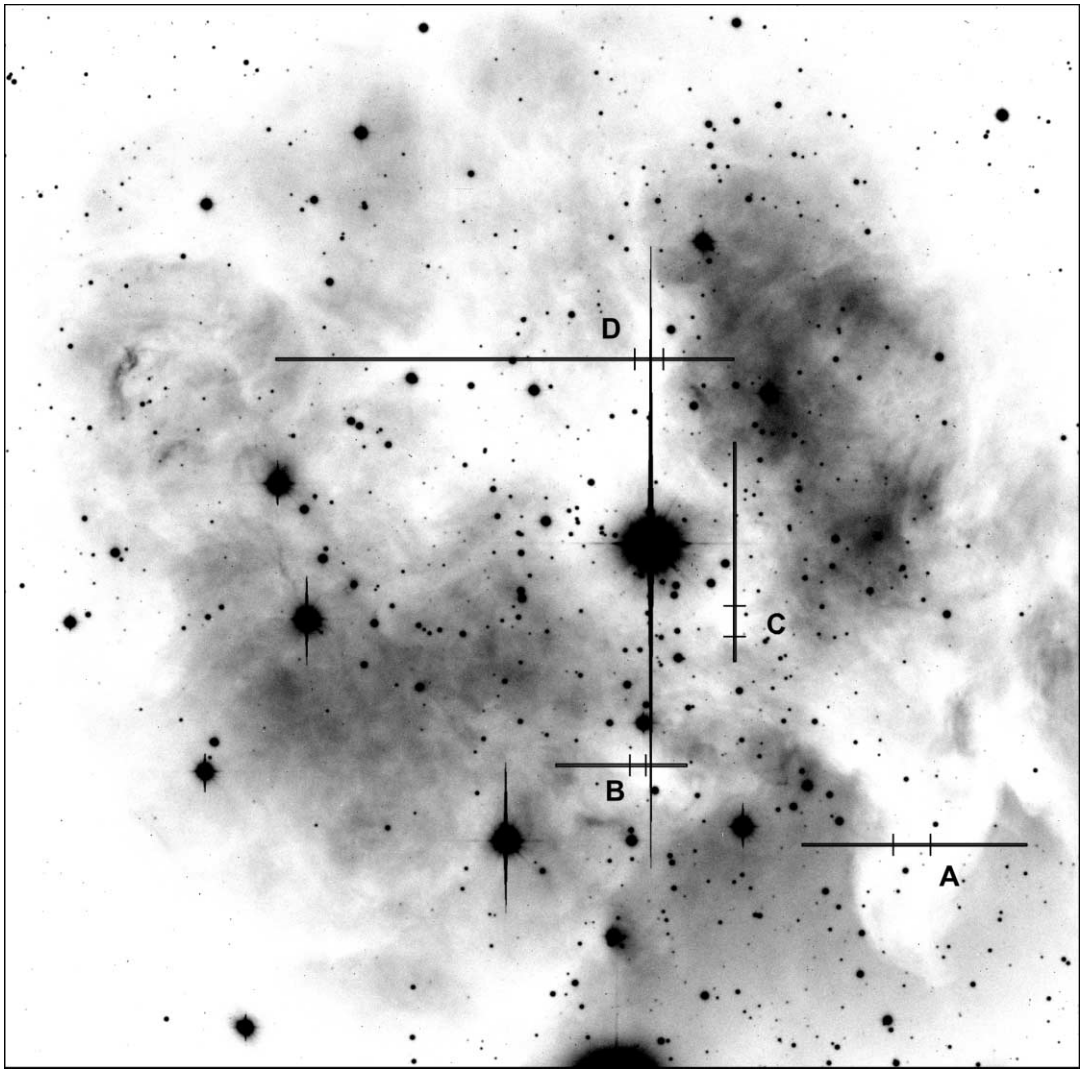

FIG. 16.—*R*-band image of IC 5146 showing the cuts across the dark lanes (see § 3.8.2) from which the extinction was inferred from the degree by which the bright background nebulosity was dimmed. The deepest section in each cut lies between the short lines, and it is from the optical depth in those segments that the *BVRI* extinctions of Table 11 were inferred.

ple, in Case I of Bodenheimer, Tenorio-Tagle, & Yorke (1979), where a hot star ($T_e \approx 40{,}000$ K) forms suddenly about 1 pc inside the near surface of a molecular cloud. After about 10^4 yr, the ionization front of the resulting H II region breaks through the front of the cloud, and the ionized material flows out through a conical volume. The expansion velocity increases outward up to about 30 km s^{-1}, and with time the apex angle of the cone opens up.

This scenario is expected to be different for IC 5146 because the exciting star has a lower temperature (30,000 to 35,000 K), and neither the effect of a finite turn-on time nor the effect of the dust that very obviously is mixed with the gas has been taken into account. However, a distance-dependent outflow velocity might be detectable.

To determine whether such an effect is present, Table 12 is a collection of the (heliocentric) velocities of the various

TABLE 11
VALUES OF EXTINCTION FOR FOUR CLOUDS

	CLOUDS				
COLOR	A ($A_\lambda \pm \sigma$)	B ($A_\lambda \pm \sigma$)	C ($A_\lambda \pm \sigma$)	D ($A_\lambda \pm \sigma$)	NORMAL A_λ / A_V
B.....	1.73 ± 0.07	1.57 ± 0.13	2.03 ± 0.16	2.57 ± 0.13	1.325
V.....	1.30 ± 0.05	1.12 ± 0.11	1.77 ± 0.11	2.16 ± 0.12	1.00
R.....	1.15 ± 0.02	0.85 ± 0.02	1.04 ± 0.02	1.29 ± 0.02	0.80
I.....	0.63 ± 0.04	0.42 ± 0.05	0.38 ± 0.03	0.79 ± 0.05	0.59
R_V.....	3.02 ± 0.62	2.49 ± 0.97	6.81 ± 5.10	5.27 ± 2.29	3.08

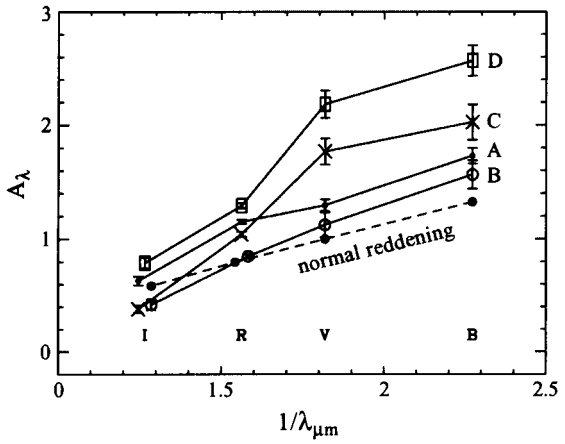

FIG. 17.—Dependence of A_λ (with respect to the background) on the effective wavelength of each passband for four points in the dark lanes of IC 5146 (some points are shifted horizontally to minimize confusion). The error bars indicate 1 σ uncertainties. The filled points and connecting dashed line represent A_λ/A_V for the normal interstellar reddening law. The values of R_V for each region are given in Table 11.

spectroscopically identifiable contributors in the line of sight to IC 5146. They become increasingly negative from cloud core toward the Sun. The velocity difference between the cloud H I and CO and the Hα emission of the H II region is 5–8 km s^{-1}, but if the -22 km s^{-1} component of the interstellar Ca II and Na I lines is formed in outflowing gas, the velocity difference at that distance from the star has increased to 16 km s^{-1}. From the asymmetric distribution of the Hα emitters with respect to +46°3474, we envisage this material expanding through a funnel pointing approximately in the direction of the Sun. The variation of Williamson's (1970) Hα velocities over the cluster might be caused by an asymmetry of the funnel with respect to the line of sight, although more detailed and accurate velocities would be needed to be certain.

Consider now the amount of material, both stellar and gaseous, in the volume of the outflow that was searched for Hα emitters. The total number of TTSs in the area of 4.8 pc^2 surveyed is 85 (including WTTSs and CTTSs, the two HH-like objects, eight "em" stars, but not the MOS detections).[6] If the survey area is assumed to be 2 pc deep, then the volume density of Hα emitters is about 9 pc^{-3}. (That quantity for IC 348 is about 60 pc^{-3}.)

The total stellar mass in IC 5146, TTSs plus those B stars that appear to be cluster members, is 64 $M_\odot$. Compare this with the amount of H II. The average electron density has been determined by Kuiper, Knapp, & Rodriguez Kuiper (1976) and by Israel (1977) from the 21 cm continuum. The two agree that $\langle n_e \rangle$ is about 60 cm^{-3} (corrected to the present distance of IC 5146), which corresponds to a H II + He mass of 18 $M_\odot$ in the ionized volume. The nebula is incompletely ionized, so the total must be somewhat higher, but it is clear that if the cluster stars are confined to that same volume, they cannot have formed from gas at the present density.

We infer that the cluster was born in a much denser region that, at that time, lay in the foreground of the present molecular cloud. Later, +46°3474 formed and cleaned out that region, but its boundaries survive in the off-center distribution of Hα emitters (Fig. 6). If the ages of the older Hα emitters in IC 5146 are to be believed, at least those stars predate the appearance of +46°3474. A population of undetected, much fainter TTSs may exist in the cloud behind +46°3474.

[6] Forte & Orsatti (1984) subtracted samplings of the stellar background outside the cluster from the number of stars brighter than $V = 20.5$ in an area of 9.′7 × 9.′7 centered on +46°3474, and so derived a total cluster population of 110 ± 20 stars. Our value of 85 stars, mostly Hα emitters but in a few cases as faint as about $V = 22.5$, refers to a smaller region (about 7′ × 7′).

TABLE 12

VELOCITIES IN THE DIRECTION OF IC 5146

Feature	$v_\odot$ (km s^{-1})	References
H I in background	−6.2	1
H I in bright nebulosity	−6 to −4	2
CO	−6 to −7	3
Stellar velocity	−4.8	4
Ca II, Na I absorption against star: component 1	−6	4
IS CH, CH^+, CN absorption against star	−7.5	4
Hα emission: at star	−14	4
Hα emission: across bright nebulosity	−8 or −11	5
H142α recombination line	−12	6
Ca II, Na I absorption against star: component 2 (foreground)	−14	4
Ca II, Na I absorption against star: component 3	−22	4

REFERENCES.—(1) Roger & Irwin 1982; (2) Roger & Irwin 1982; the velocities given enclose the peak emission; fainter H I emission is present between −9 and −2 km s^{-1}; see their Fig. 6. (3) Lada & Elmegreen 1979; McCutcheon et al. 1982; Dobashi et al. 1992; the CO and the FIR (Sargent et al. 1981; Wilking et al. 1994) emission is concentrated in three extended regions differing about 1.5 km s^{-1} in velocity. (4) This paper. (5) The mean Hα velocity from Williamson's (1970) sampling is −10.9 km s^{-1}, with a scatter of about 5 km s^{-1} on either side of the mean. Georgelin & Georgelin (1970) give a mean of −8.3 km s^{-1} with a rms of 4.4 km s^{-1}, presumably from the scatter of their 39 points distributed over a field 20′ in diameter. (6) Kuiper et al. (1976): this is the mean velocity averaged over a beam width of 8.′1; it samples the entire ionized volume.

FIG. 18.—False-color direct image of the BD +46°3471 region (assembled from *B*-, *V*-, and *I*-band frames), with arrows indicating Hα-emission stars. The two close companions of +46°3471 discussed in § 4.1 are lost in the overexposed images of that star, but the position of the southwestern Hα emitter (IHα-177) is marked with a black dot. The area shown is about 7′ on a side, with north at the top and east to the left. It can be identified in Fig. 1.

4. THE BD +46°3471 REGION

4.1. *The Vicinity of BD +46°3471*

BD +46°3471 is slightly variable (it is V1578 Cyg) and illuminates a reflection nebula, shown in Figures 1 and 18, that does not seem to have been commented on before. The star has two faint companions mentioned by Walker (1959). They were measured in *JHK* by Li et al. (1994) and denoted *a* and *b*. Star *b* (No. 534 in Table 2) was also seen by Pirzkal, Spillar, & Dyck (1997). The two lie at approximately the same distance on opposite sides of +46°3471: *b* at 5″.1 in P.A. 37°, *a* at 5″.5 in 205°. Both stars are readily observable at shorter wavelengths. Hα is in emission in *a* (No. 531 = IHα-177 in Table 2), but the star is a close double with a separation about 0″.6, and it is not apparent in which component the Hα emission originates. LkHα-236 is a more distant companion, lying about 15″ to the west. Zinnecker & Preibisch (1994) detected +46°3471 in a *ROSAT* survey of HAeBe stars, but one of its close companions may be the actual X-ray source. This could be checked by X-ray imaging at higher angular resolution.

This region is notably poorer in emission-Hα stars than IC 5146. They are marked by arrows in Figure 18. It is striking how many are concentrated in the grouping centered on +46°3471.

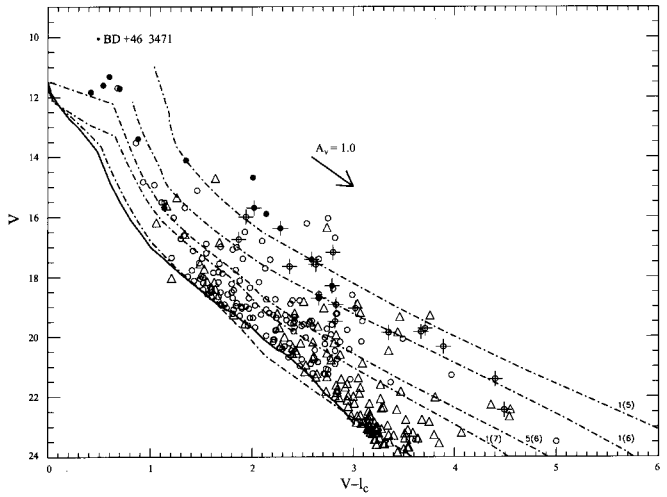

FIG. 19.—V, $V-I$ diagram for the BD +46°3471 region, not corrected for reddening. Filled circles are objects of known spectral type. Open circles represent stars of unknown type with undetectable Hα emission. Unfilled triangles denote stars either too faint to detect emission, or which lie outside the grism survey area. The dot near the top represents +46°3471.

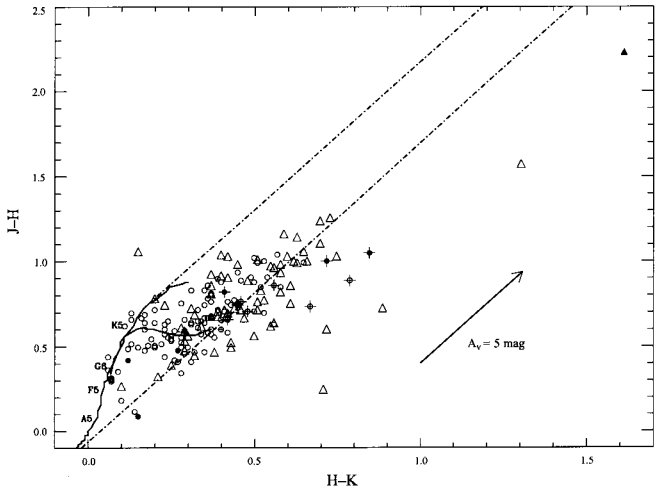

FIG. 20.—$J-H$, $H-K$ diagram for stars in the BD +46°3471 region. The symbols are as in Fig. 19.

4.2. *Color-Magnitude Diagram*

Figure 19 is a plot of the *observed* V, $V-I$ for all the stars in the BD +46°3471 region believed to lie above the main sequence. No allowance has been made for reddening on account of the paucity of stars of known spectral type in the field. The dot near the top represents +46°3471. The bright F- and G-type stars W8, W9, W11, and W14 are probably in the foreground because of their low A_V values. Many of the 300 stars listed in Table 2 must be interlopers for the reasons discussed in § 3.2. In addition, the rapidly increasing star density to the southwest of +46°3471 suggests that it lies near the cloud edge, so that additional contamination by K and M giants in the background is a concern. If one simply assumes that the distance and mean A_V of IC 5146 apply to the 18 Hα emitters around +46°3471, then the DM97 isochrones lead to a median log age of 5.3. Similarly, the median log age is 7.27 for all the 250 stars above the main sequence.

Figure 20 is the $J-H$, $H-K$ diagram for the +46°3471 field. Most stars lie within the normal reddening band. The Hα emitters that lie to the right of the reddening band are all CTTSs, but two stars with strong Hα emission do not (Nos. 444 and 597).

One interesting object is a bright infrared source lying 19.″2 east of LkHα-239. It is a close binary whose optical counterpart is just visible in Figure 18. The coordinates and color of the primary are given as IR-7 in Table 10. The secondary is 1.″9 northwest of the primary and is about 1.5 mag fainter in K. This object is nearly as bright as the Wilking et al. (1984) source near the southeast CO/FIR peak of IC 5146. No other comparable IR source is evident in the +46°3471 field. It is plotted as a filled triangle in Figure 20.

4.3. *The Spectrum of BD +46°3471*

BD +46°3471 is one of the original HAeBe stars (Herbig 1960b), and since that time the optical spectrum has been studied by Finkenzeller & Mundt (1984), who give references to earlier work, and Finkenzeller & Jankovics (1984), Hamann & Persson (1992), and Bouret & Catala (1998). This is not the place to describe or interpret the spectrum in detail, but a few remarks are in order, if only to emphasize the great difference between the spectra of +46°3471 and BD +46°3474 (§ 3.8), of about the same brightness and involved in the same cloud only 10′ apart.

The spectrum of +46°3471 as observed with HIRES on 2000 November 5 is complex: a rotationally broadened, early-type absorption spectrum (classified as A0 III by Gray & Corbally 1998) upon which are superposed strong emission lines of H and the ionized metals. The P Cyg emission at Hα degrades down the series to a weak, nearly central emission core in the broad A-type absorption lines. The central emission in stellar Ca II λ3933 is shown in the top left panel of Figure 21. Similar emission is present in the Na I D_{12} lines. The Hα and Ca II structure is variable with time according to Catala, Czarny, & Felenbok (1988).

The absorption lines are not quite symmetric: as noted by others, the longward wing is somewhat the more extended; this is seen clearly in the Ca II profile in Figure 21. Nevertheless an approximate representation of the structure of the Fe II and Ti II lines can be made by adding to a rotationally broadened absorption line (the asymmetry ignored) a simple Gaussian emission core, and adjusting the widths, strengths, and centers for best fit. Three panels of Figure 21 show such fits to Fe II λ5018 and λ5236 and Ti II λ4443, lines chosen for freedom from blends. The filled points show the observed points, the dotted lines the separate outlines of the absorption and emission components, and the solid line their simple sum. The caption to Figure 21 gives the FWHM of the Gaussian emissions and the $v \sin i$ of the absorptions. The latter averages about 180 km s^{-1}, as compared to 150 km s^{-1} from Böhm & Catala (1995).

There is probably weak P Cyg structure present in all of these lines, suggested by the departure of the observations from the fit at the shortward side of the absorption core. The λ5018 line also has an unexplained secondary peak at about -200 km s^{-1}, noted also by Bouret & Catala (1998). This is not He I λ5015 because other strong Fe II lines of multiplets RMT 42 and 49 show the same feature, and because other He I emission lines elsewhere in this spectrum are weak or absent.

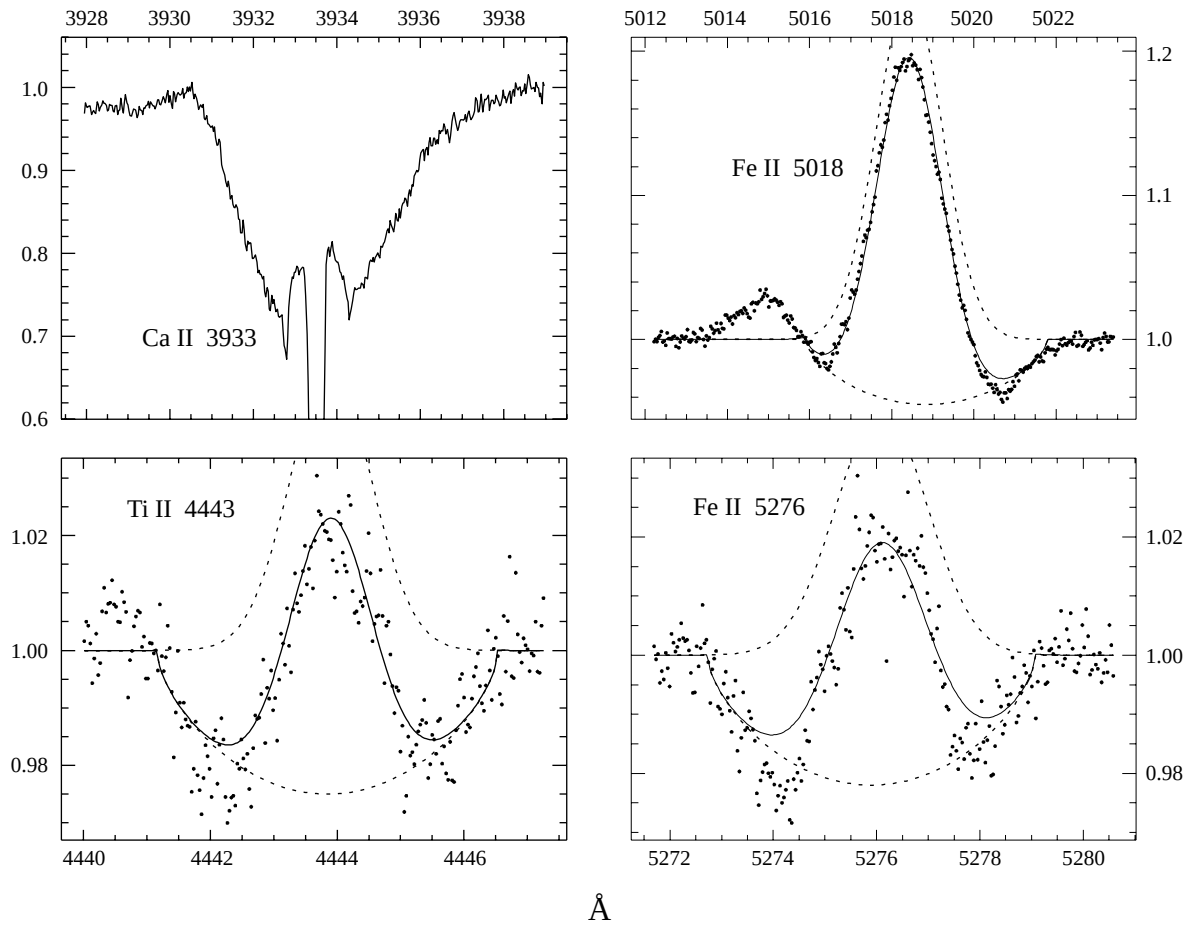

FIG. 21.—*Top left*: Ca II λ3933 line in BD +46°3471, showing the emission core (its center cut out by the off-scale interstellar line) superposed on the broad absorption line of the A0 star. The secondary peak at on the shortward edge is real, and is seen at other strong lines, as is the absorption wing asymmetry. *Top right:* The profile of Fe II λ5018. The filled points are the observations and the solid line is the fit to them by the sum of a rotationally broadened absorption line ($v \sin i = 175$ km s^{-1}) and a Gaussian emission component (FWHM = 100 km s^{-1}), shown as dotted lines. As at λ3933, the secondary peak on the shortward edge is real. *Bottom left:* The profile of Ti II λ4443, represented in the same way. Here, $v \sin i = 180$ km s^{-1}, and the emission FWHM = 104 km s^{-1}. *Bottom right:* Fe II λ 5276 represented in the same way, with $v \sin i = 180$ km s^{-1} and emission FWHM = 120 km s^{-1}.

The radial velocity of +46°3471 is expected to be near that of its molecular cloud, which is $v_{\odot} = -6.9$ km s^{-1} (Scappini et al. 1994), but direct determination is precluded by the complexity of the spectrum. Corporon & Lagrange (1999) found no velocity variations but gave no mean velocity. The absorption lines are too broad and confused by emission on our spectrograms to provide a reliable velocity, while velocities from emission lines depend upon line strength. Weak to moderately intense Fe II, Ti II, and Sc II lines at $\lambda > 4300$ Å average +9 km s^{-1}, while the strongest Fe II lines and those of Ti II near 3700 Å give −1 km s^{-1}.

The three HH objects near BD +46°3471 discovered by Goodrich (1993) on narrowband direct images also appear on the grism spectrograms. The [S II] blend is present in the two brightest (Goodrich's HH1 and HH2). All three are fainter than those near BD +46°3474 (§ 3.7) but differ in being very obviously nonstellar. Although broadband magnitudes of such nearly monochromatic sources are not very meaningful, *R* magnitudes are useful in a differential sense: they are 20.7, 21.3, and 21.5 for HH1, HH2, and HH3, respectively, as compared with 19.0 and 19.1 for the two in IC 5146. The difference probably is due to the stars that contribute to the IC 5146 objects.

5. FINAL REMARKS

Here is a summary of the more interesting results and unanswered questions that have emerged from this investigation.

1. Our observations support an earlier suggestion by Roger & Irwin (1982) that the formation of BD +46°3474, type B0 V and the most luminous member of the IC 5146 cluster, created a blister in the front surface of the molecular cloud, and that gas is now streaming outward approximately in the direction of the Sun. Radial velocities obtained from various constituents of the neutral and ionized gas indicate that the outflow velocity increases with distance from the star, as predicted in some champagne models.

About 100 stars having Hα in emission and brighter than about $R = 20.5$ are now known in and around IC 5146 (some 80 having been discovered during this investigation). Following correction for extinction and assuming a distance of 1.2 kpc (inferred from three late B-type cluster members), these stars are found to lie in a band elevated above the ZAMS, as expected for a population of young, low-mass, pre–main-sequence stars. A representative age is 1 Myr, but

a precise value for the median age and its dispersion depends heavily upon whose evolutionary tracks are used to interpret the photometry.

The distance of 1.2 kpc for IC 5146 means that the true cluster population is diluted by a significant contribution from the foreground. Simplified assumptions as to the foreground extinction and star density suggest that a substantial fraction of the stars above the main sequence in the V_0, $(V-I)_0$ color-magnitude diagram are foreground interlopers. Thus IC 5146 is hardly a suitable object to elucidate the perennial question, do young pre–main-sequence stars with little or no emission exist in this mass range?

2. The mass tied up in certifiable cluster members, about 64 $M_\odot$, is much greater than the amount of H II + He in the H II region, about 18 $M_\odot$. From this disparity we infer that the cluster was formed in a dense section of the present molecular cloud that originally lay in front of IC 5146, but that has now been largely dissipated following the formation of +46°3474, the opening up of the blister, and the subsequent outflow. The bright nebulosity of IC 5146 is symmetrically distributed around +46°3474, but the Hα emitters are not: there is a conspicuous lack of such stars on the west and northwest of the nebula (Fig. 6). This off-center distribution of TTSs may outline the boundaries of that original cloud.

3. Since data now exist for the emission-Hα stars in both IC 5146 and the nearer (about 320 pc) young cluster IC 348, the properties of the two populations can be compared. Down to the same limit in M_V (+7.6) and Hα equivalent width (3 Å), the surface density (per square parsec) of Hα emitters is higher in IC 348 than in IC 5146 by a factor of 2.5. There is a clear difference in the frequency distributions of W(Hα): the fraction of Hα emitters above the 3 Å detection threshold that are WTTSs is 0.52 ± 0.12 in IC 348 and only 0.23 ± 0.06 in IC 5146. Whether the preponderance of WTTSs in IC 348 is an effect of age we cannot say. Future grism observations of young clusters will clarify this issue.

Two objects in IC 5146 that at first appeared to be stars were found to have very strong emission lines of [S II], [N II], [O I], ... that are characteristic of HH objects. One shows in addition to the HH forbidden lines a strong continuous spectrum and permitted lines, typical of ordinary T Tauri stars. This object is slightly nonstellar at the 1″–2″ level. Its forbidden lines are shifted about 200 km s^{-1}, with opposite signs on opposite sides of the star. These two objects lie about 25″ apart, very near +46°3474; it is not apparent whether they have any direct connection with that star.

4. The HAeBe star BD +46°3471 lies in the same molecular cloud about 10′ (3.5 pc in projection) west of +46°3474 and illuminates a small reflection nebula of its own (see Fig. 1, which shows them both). The two are about the same apparent magnitude, yet their spectra and local circumstances are very different. The source of the illumination of IC 5146, +46°3474, has a normal B0 V spectrum with very narrow lines ($v \sin i = 10$ km s^{-1}), apparently a constant radial velocity, no obvious IR excess, and is the brightest of a cluster of over 100 stars. On the other hand, +46°3471 is variable in light, has a complex emission spectrum, a major IR excess plus a peculiar optical region color, rapid rotation ($v \sin i \approx 180$ km s^{-1}), and is accompanied by only a minor clustering of T Tauri stars.

Why such a difference? It is possible that once +46°3471 reaches the main sequence some of its abnormalities will have disappeared, its temperature will have risen, and it might have some effect on the structure of the surrounding cloud. But why should a large cluster of lower mass stars already have formed around +46°3474 and only a very minor grouping at +46°3471? New molecular-line observations are recommended.

We are indebted to the National Science Foundation for partial support of this investigation under grant AST 97-30934. We also thank Brian Patten and Marni Krismer for their contributions and help during the early stages of this investigation and John Tonry for obtaining spectra of the two suspected HH objects in IC 5146.

REFERENCES

Adams, W. S. 1949, ApJ, 109, 354
Allen, L. E., & Strom, K. M. 1995, AJ, 109, 1379
Baraffe, I., Chabrier, G., Allard, F., & Hauschildt, P. H. 1998, A&A, 337, 403 (B98)
Blaauw, A. 1963, in Basic Astronomical Data, ed. A. Blaauw & M. Schmidt (Chicago: Univ. Chicago Press), 383
Bodenheimer, P., Tenorio-Tagle, G., & Yorke, H. W. 1979, ApJ, 233, 85
Böhm, T., & Catala, C. 1995, A&A, 301, 155
Bouret, J.-C., & Catala, C. 1998, A&A, 340, 163
Briceño, C., et al. 2001, Science, 291, 93
Carpenter, J. M., Meyer, M. R., Dougados, C., Strom, S. E., & Hillenbrand, L. A. 1997, AJ, 114, 198
Catala, C., Czarny, J., & Felenbok, P. 1988, in IAU Symp. 132, The Impact of Very High S/N Spectroscopy on Stellar Physics, ed. G. Cayrel de Strobel & M. Spite (Dordrecht: Kluwer), 105
Catala, C., Czarny, J., Felenbok, P., & Praderie, F. 1986, A&A, 154, 103
Corporon, P., & Lagrange, A.-M. 1999, A&AS, 136, 429
Couteau, P. 1987, A&AS, 67, 13
Crampton, D., & Fisher, W. A. 1974, Publ. DAO, 14, 283
D'Antona, F., & Mazzitelli, I. 1997, in Cool Stars in Clusters and Associations, ed. G. Micela & R. Pallavicini (Firenze: Soc. Astron. Italiana), 807 (DM97)
Dobashi, K., Yonekura, Y., Mizuno, A., & Fukui, Y. 1992, AJ, 104, 1525
Elias, J. H. 1978, ApJ, 223, 859
Finkenzeller, U., & Jankovics, I. 1984, A&AS, 57, 285
Finkenzeller, U., & Mundt, R. 1984, A&AS, 55, 109
Forte, J. C., & Orsatti, A. M. 1984, ApJS, 56, 211
Georgelin, Y. P., & Georgelin, Y. M. 1970, A&A, 7, 332
Gies, D. R., & Lambert, D. L. 1992, ApJ, 387, 673
Gómez, A. E., Luri, X., Mennessier, M. O., Torra, J., & Figueras, F. 1997, in *Hipparcos* Venice 1997, ed. B. Battrick, M. A. C. Perryman, & P. L. Bernacca (ESA SP-402) (Noordwijk: ESA), 207
Goodrich, R. W. 1993, ApJS, 86, 499
Gray, R. O., & Corbally, C. J. 1998, AJ, 116, 2530
Haisch, K. E., Lada, E. A., & Lada, C. J. 2001, AJ, 121, 2065
Hamann, F., & Persson, S. E. 1992, ApJS, 82, 285
Hartmann, L. 1998, Accretion Processes in Star Formation (Cambridge: Cambridge Univ. Press)
———. 2001, AJ, 121, 1030
Herbig, G. H. 1960a, ApJ, 131, 516
———. 1960b, ApJS, 4, 337
———. 1995, ARA&A, 33, 19
———. 1998, ApJ, 497, 736
Herbig, G. H., Vrba, F. J., & Rydgren, A. E. 1986, AJ, 91, 575
Hughes, J., Hartigan, P., Krautter, J., & Klemen, J. 1994, AJ, 108, 1071
Hunt, L. K., Mannucci, F., Testi, L., Migliorini, S., Stanga, R. M., Baffa, C., Lisi, F., & Vanzi, L. 1998, AJ, 115, 2594
Israel, F. P. 1977, A&A, 60, 233
———. 1978, A&A, 70, 769
Jacoby, G. H., Hunter, D. A., & Christian, C. A. 1984, ApJS, 56, 257
Jahreiss, H., & Wielen, R. 1997, in *Hipparcos* Venice 1997, ed. B. Battrick, M. A. C. Perryman, & P. L. Bernacca (ESA SP-402) (Noordwijk: ESA Publications Division), 675
Jaschek, C., & Gómez, A. E. 1998, A&A, 330, 619
Johnson, H. L., & Hiltner, W. A. 1956, ApJ, 123, 267
Kenyon, S. J., & Hartmann, L. 1995, ApJS, 101, 117
Kilian, J. 1992, A&A, 262, 171
Kirkpatrick, J. D., Henry, T. J., & McCarthy, D. W. 1991, ApJS, 77, 417

Kroupa, P. 1995, ApJ, 453, 358
Kuiper, T. B. H., Knapp, G. R., & Rodriguez Kuiper, E. N. 1976, A&A, 48, 475
Lada, C. J., & Elmegreen, B. G. 1979, AJ, 84, 336
Lada, C. J., Lada, E. A., Clemens, D. P., & Bally, J. 1994, ApJ, 429, 694
Lada, E. A., & Lada, C. J. 1995, AJ, 109, 1682
Landolt, A. U. 1992, AJ, 104, 340
Leggett, S. K., Allard, F., Dahn, C., Hauschildt, P. H., Kerr, T. H., & Rayner, J. 2000, ApJ, 535, 965
Leggett, S. K., Allard, F., & Hauschildt, P. H. 1998, ApJ, 509, 836
Li, W., Evans, N. J., Harvey, P. M., & Colomé, C. 1994, ApJ, 433, 199
Liu, T., Janes, K. A., & Bania, T. M. 1989, AJ, 98, 626
———. 1991, AJ, 102, 1103
Lynds, B. T., & O'Neil, E. J., Jr. 1985, ApJ, 294, 578
McCutcheon, W. H., Roger, R. S., & Dickman, R. L. 1982, ApJ, 256, 139
Münch, G. 1957, ApJ, 125, 42
O'Tuairisg, S., Cami, J., Foing, B. H., Sonnentrucker, P., & Ehrenfreund, P. 2000, A&AS, 142, 225
Palla, F., & Stahler, S. 1999, ApJ, 525, 772 (PS99)
Pirzkal, N., Spillar, E. J., & Dyck, H. M. 1997, ApJ, 481, 392
Roger, R. S., & Irwin, J. A. 1982, ApJ, 256, 127
Sargent, A. I., van Duinen, R. J., Fridlund, C. V. M., Nordh, H. L., & Aalders, J. W. G. 1981, ApJ, 249, 607
Scappini, F., Palumbo, G. G. C., Bruni, G., & Bergman, P. 1994, ApJ, 427, 259
Schmidt-Kaler, T. 1982, in Landolt-Börnstein, New Series, Group 6, Vol. 2b, Stars and Star Clusters, ed. K. Schaifers & H. H. Voight (Berlin: Springer), 10
Siess, L., Dufour, E., & Forestini, M. 2000, A&A, 358, 593 (S00)
Straižys, V. 1992, Multicolor Stellar Photometry (Tucson: Pachart)
Walborn, N. R., & Fitzpatrick, E. L. 1990, PASP, 102, 379
Walker, M. F. 1959, ApJ, 130, 57
White, G. J., et al. 1999, A&A, 342, 233
Wilking, B. A., Harvey, P. M., & Joy, M. 1984, AJ, 89, 496
Williamson, R. A. 1970, Ap&SS, 6, 45
Zinnecker, H., & Preibisch, Th. 1994, A&A, 292, 152